JOURNAL OF GEOPHYSICAL RESEARCH, VOL. 104, NO. D15, PAGES 18,841–18,866, AUGUST 20, 1999

# Polar vortex dynamics during spring and fall diagnosed using trace gas observations from the Atmospheric Trace Molecule Spectroscopy instrument

G. L. Manney,[1] H. A. Michelsen,[2] M. L. Santee,[1] M. R. Gunson,[1] F. W. Irion,[1] A. E. Roche,[3] and N. J. Livesey[1]

**Abstract.** Trace gases measured by the Atmospheric Trace Molecule Spectroscopy (ATMOS) instrument during three Atmospheric Laboratory for Applications and Science (ATLAS) space-shuttle missions, in March/April 1992 (AT-1), April 1993 (AT-2), and November 1994 (AT-3) have been mapped into equivalent latitude/potential temperature (EqL/θ) coordinates. The asymmetry of the spring vortices results in coverage of subtropical to polar EqLs. EqL/θ fields of long-lived tracers in spring in both hemispheres show the net effects of descent at high EqL throughout the winter, reflecting strong descent in the upper stratosphere, decreasing descent at lower altitudes, and evidence of greater descent at the edge of the lower stratospheric vortex than in the vortex center; these results are consistent with trajectory calculations examining the history of the air measured by ATMOS in the month prior to each mission. EqL/θ tracer fields, the derived fields $CH_4$-$CH_4^*$ ($CH_4^*$ is the expected $CH_4$ calculated from a prescribed relationship with $N_2O$ for fall) and $NO_y$-$NO_y^*$ (analogous to $CH_4^*$), and parcel histories all indicate regions of strong mixing in the 1994 Southern Hemisphere (SH) spring vortex above 500 K, with the strongest mixing confined to the vortex edge region between 500 and 700 K, and mixing throughout the Northern Hemisphere (NH) spring vortex in 1993 below about 850 K. Parcel histories indicate mixing of extravortex air with air near the vortex edge below 500 K in the SH but not with air in the vortex core; they show extravortex air mixing well into the vortex above ~450 K in the NH and into the vortex edge region below. The effects of severe denitrification are apparent in EqL/θ $HNO_3$ in the SH lower stratospheric spring vortex. The morphology of $HNO_3$ in the Arctic spring lower stratospheric vortex is consistent with the effects of descent. EqL/θ fields of ATMOS $NO_y$-$NO_y^*$ show decreases consistent with the effects of mixing throughout the NH lower stratospheric vortex. The EqL/θ-mapped ATMOS data thus indicate no significant denitrification during the 1992-1993 NH winter. Examination of $H_2O$+2$CH_4$ shows that dehydration in SH spring 1994 extended up to ~600 K; it also suggests the possibility of a small amount of dehydration in the NH 1993 spring vortex below ~465 K. Ozone depletion is evident in the spring vortices in both hemispheres. Differences in autumn EqL/θ tracer fields between the missions reflect the fact that each succeeding mission took place ~2 weeks later in the season, when the vortex had developed further. There was greater average descent and greater isolation of air in the developing vortex during each succeeding mission, consistent with progressively larger downward excursions of long-lived tracer contours observed in the upper stratosphere at high EqL.

## 1. Introduction

The space-shuttle-borne Atmospheric Trace Molecule Spectroscopy (ATMOS) instrument is a high-resolution Fourier transform infrared spectrometer that operates in solar occultation mode and simultaneously measures vertical profiles of ~30 species. During the three Atmospheric Laboratory for Applications and Science (ATLAS) missions in March/April 1992 (AT-1), April 1993 (AT-2), and November 1994 (AT-3), ATMOS observed midlatitudes and the subtropics during two austral (AT-1 and AT-2) and one boreal (AT-3) autumn and high latitudes in and around the decaying polar vortex in one austral (AT-3) and one boreal (AT-2) spring, as well as the tropics during AT-1 and AT-3 [*Gunson et al.*, 1996].

Several studies have explored aspects of vortex versus extravortex conditions in spring using AT-2 and/or AT-3

[1]Jet Propulsion Laboratory, California Institute of Technology, Pasadena.
[2]Atmospheric and Environmental Research, Inc., San Ramon, California.
[3]Lockheed Martin Advanced Technology Center, Palo Alto, California.



Paper number 1999JD900317.
0148-0227/99/1999JD900317$09.00

ATMOS data. Although both AT-2 and AT-3 observations in the spring hemisphere were taken in a narrow band at high latitudes, since the polar vortex is strongly distorted and air is frequently drawn up from low latitudes in spring, these observations sampled both vortex and extravortex air [e.g., *Manney et al.*, 1996b]. *Abrams et al.* [1996a, c] used long-lived tracer observations inside and outside the Antarctic and Arctic polar vortices to quantitatively estimate vortex-averaged descent over the winter. *Rinsland et al.* [1995, 1996a, b, 1999] compared vortex and extravortex ATMOS observations of chlorine, nitrogen, and hydrogen species.

*Michelsen et al.* [1998a] used $N_2O$ and $CH_4$ data from the three ATLAS missions to show that there existed tight but distinct correlations between the two tracers in the tropics, the springtime vortex, and the extravortex/extratropics regions. The existence of distinct compact correlation curves is helpful in diagnosing mixing between air masses across "transport barriers" (such as the polar vortex edge) [e.g., *Waugh et al.*, 1997]. *Michelsen et al.* [1998b] used correlations of $N_2O$ with $NO_y$ and $O_3$ and estimates of mixing from $N_2O$ and $CH_4$ to quantitatively estimate denitrification and chemical ozone loss in the Arctic and Antarctic spring vortices.

It has also been shown that, although the fall measurements from the ATLAS missions only extended up to ~50° latitude [*Gunson et al.*, 1996], the developing polar vortices (the "protovortices") were sufficiently variable [e.g., *Manney et al.*, 1996b] that air from within them was sampled; tracer correlations for this air are distinct from those for midlatitude air [*Michelsen et al.*, 1998b].

Although these previous studies show that a variety of conditions were sampled by ATMOS during the ATLAS missions despite limited spatial and temporal coverage, the full extent of the coverage of meteorological conditions was not realized in these studies, since the observations were grouped in a few broad categories (e.g., vortex and extravortex or tropics and midlatitudes). Longitudinal cross sections [*Abrams et al.*, 1996a, c; *Rinsland et al.*, 1996a, b, 1999] do not give a clear picture of the relative position of observations away from the vortex edge and even blur the vortex boundary, since the position of the vortex and latitude of observations changed during the missions.

A useful tool for displaying sparse data and diagnosing the effects of dynamical and chemical processes on trace gas distributions is to map them on isentropic (constant potential temperature, $\theta$) surfaces (along which air moves in the absence of diabatic effects) as a function of potential vorticity (PV) [e.g., *Schoeberl et al.*, 1989, 1992; *Manney et al.*, 1994b] or equivalent latitude (the latitude that would enclose the same area as the corresponding PV contour) [e.g., *Butchart and Remsberg*, 1986; *Schoeberl et al.*, 1995; *Lary et al.*, 1995].

In the following, we present an overview of ATMOS observations from the three ATLAS missions mapped into equivalent latitude (EqL)/$\theta$ space. We focus on long-lived tracers (e.g., $N_2O$ and $CH_4$) whose distributions provide information on transport and mixing; distributions of other species (e.g., $O_3$ and $HNO_3$) that have good EqL/$\theta$-space coverage and derived quantities that are useful in diagnosing mixing and/or chemical processes are also shown. To aid in interpretation of these results, we also show air parcel histories from back trajectory calculations for the ATMOS observation locations. The EqL/$\theta$ mapping provides a common coordinate system based on the meteorological conditions under which the measurements were taken, allowing detailed comparisons between trace gas distributions for the three missions. We show detailed comparisons between the springtime Arctic and Antarctic vortices and between the developing vortices in fall. ATMOS data have not previously been presented in EqL/$\theta$ space, and our results provide new information on the details and spatial distribution of the effects of transport and mixing processes and the interplay between these processes and polar vortex chemistry in the lower stratosphere.

## 2. Meteorological Conditions During the ATLAS Missions

The ATMOS data cover March 25–April 2, 1992 (AT-1), April 8–16, 1993 (AT-2), and November 3–12, 1994 (AT-3). Table 1 summarizes the spatial coverage of the version 2 data used here; the coverage is shown in more detail by *Gunson et al.* [1996]. AT-3 and AT-2 sunrise observations were made at high latitudes in the Southern Hemisphere (SH) and Northern Hemisphere (NH) spring, respectively; AT-1 sunrise observations were in the tropics. Sunset observations from all three missions were in the fall when the polar vortex was developing, in the NH during AT-3 and in the SH during AT-2 and AT-1.

Meteorological data (temperature, geopotential height, horizontal wind) from the U.K. Meteorological Office (UKMO) troposphere-stratosphere data assimilation system

**Table 1.** ATMOS Coverage During the ATLAS Missions

| Mission | Dates | Sunrise/ Sunset | Seasonal Conditions | Latitude Coverage | Number of Profiles | Longitude Distribution |
|---|---|---|---|---|---|---|
| AT–3 | November 3-12, 1994 | SR | spring | 72.4°S–64.5°S | 81 | approximately uniform |
| | | SS | fall | 3.4°N–49.2°N | 96 | approximately uniform |
| AT–2 | April 8-16, 1993 | SR | spring | 63.5°N–69.1°N | 61 | approximately uniform |
| | | SS | fall | 50.2°S–27.0°S | 34 | sparse ~ 60° to 180°E |
| AT–1 | March 25-April 2, 1992 | SR | tropics | 28.2°S–30.5°N | 45 | sparse ~ -60° to 80°E |
| | | SS | fall | 55.5°S–21.9°S | 39 | none ~ -180° to -110°E |

[*Swinbank and O'Neill*, 1994] were used to calculate PV and "scaled PV" and analyzed to provide a meteorological context for the ATMOS observations. Scaled PV (sPV) is in "vorticity units" [*Dunkerton and Delisi*, 1986], as described by *Manney et al.* [1994c]. The UKMO data are provided on the Upper Atmosphere Research Satellite (UARS) standard pressure levels (six levels per decade in pressure or about 2.5 km vertical spacing) extending up to 0.316 hPa (~2300–2500 K) but are not considered as reliable in the top few levels. Reliable and complete PV fields can thus be calculated up to ~2000 K.

Plate 1 summarizes the meteorological conditions in the spring hemisphere during AT-3 and AT-2, showing |sPV| maps with temperature contours overlaid at representative levels in the middle and lower stratosphere, averaged over 8 days during AT-3 and AT-2. The latitude bounds of the ATMOS observations are indicated. The longitudinal position of the vortex remained sufficiently constant during each mission that these maps give a representative picture [e.g., *Manney et al.*, 1996b], although the extrema of PV values are smoothed out. The vortex is demarked by a region of strong sPV gradients that occurs at different |sPV| values for varying dynamical situations. Comparison of the steepness of the sPV gradients between Plates 1a and b or Plates 1c and d gives an indication of the relative strength of the Antarctic and Arctic vortices at the levels shown. The Antarctic vortex is stronger throughout the winter than the Arctic vortex; it also breaks down later, especially in the lower stratosphere [e.g., *Manney et al.*, 1994c, and references therein]. Thus the vortex was larger and stronger at both levels during AT-3 than during AT-2, although AT-3 was ~2 weeks later in spring than AT-2.

The polar vortex in the SH typically breaks down starting at the top, and the erosion is relatively gradual; although tongues of material are drawn off of the vortex, they are not generally so large that an individual tongue represents a substantial portion of the vortex [e.g., *Manney et al.*, 1994c]. As these tongues are drawn out, air is also drawn in around the vortex edge from low latitudes, with $|\mathrm{sPV}| \lesssim 0.6 \times 10^{-4}\ \mathrm{s}^{-1}$ (subtropical values) observed at the latitudes sampled by ATMOS. Plate 1a shows that during AT-3 there was still a well-defined (although weaker and smaller than in midwinter) vortex in the SH middle stratosphere; distinct vortex remnants were present at levels up to ~1300 K [*Manney et al.*, 1996b; *Abrams et al.*, 1996a].

As seen in Plate 1b, the situation in the Arctic middle stratosphere is more complicated. The Arctic vortex was in the midst of breaking down in a more rapid and dramatic manner than in the SH. At the beginning of AT-2, a huge tongue of vortex air had been drawn out, representing a significant fraction of the vortex area. As the mission progressed, this tongue of vortex air was drawn farther out and, starting about April 13, 1993, wrapped back upon itself around the anticyclone over the pole, so that a cross section of the hemisphere from 90° to 270°E over the pole would show vortex air in three places: in the main vortex remnant along 90°E at ~60-80°N, in the tail of the drawn-out tongue over the pole, and in the main part of the tongue along 270°E at ~30-50°N. Low-PV air was drawn up between the vortex and the tongue into the anticyclone and coiled up with the tongue of vortex air. On individual days, ATMOS could have sampled vortex air in two or three places, in addition to midlatitude air ($\mathrm{sPV} \lesssim 0.9 \times 10^{-4}\ \mathrm{s}^{-1}$). The average in Plate 1b shows a broader tongue and higher sPV values between the main vortex and the tongue than on the individual days, as the shape and position of the tongue changed significantly during the mission. This tongue extended from ~700–1100 K. Above that level, the polar vortex had already dissipated.

During AT-3 a summer-like temperature pattern was already present in the SH middle and upper stratosphere, with high temperatures centered over the pole. In contrast, during AT-2 the Arctic middle stratosphere had not completed this transition and temperatures at 840 K were nearly constant, with slightly higher temperatures appearing at high latitudes.

In the lower stratosphere the SH vortex during AT-3 was still strong and only slightly smaller than its midwinter dimensions [*Manney et al.*, 1996b]; the Antarctic lower stratospheric vortex typically remains intact into December [*Manney et al.*, 1994c]. In contrast, the NH lower stratospheric vortex during AT-2 was much smaller than in midwinter but still defined by strong PV gradients. The Arctic lower stratospheric vortex during the 1992-1993 winter was the strongest on record [*Manney et al.*, 1994a; *Zurek et al.*, 1996]; *Manney et al.* [1994a] and *Dahlberg and Bowman* [1995] showed that this led to substantially less exchange across the vortex edge than is usual in the Arctic. The lower stratospheric vortex (defined by the region of strong PV gradients) was delimited by higher |sPV| values in the NH than in the SH: |sPV| values near $1 \times 10^{-4}\ \mathrm{s}^{-1}$ were representative of the vortex edge in the austral lower stratosphere but represented midlatitude conditions in the boreal lower stratosphere. This is consistent with the NH final warming being more advanced, since the region of strong PV gradients typically shifts to higher PV values as the vortex erodes [e.g., *Manney et al.*, 1994a; *Waugh and Randel*, 1999]. In both hemispheres the lower stratospheric vortices were eroded mainly via small filaments drawn off the vortex and stretched out into midlatitudes, where they eventually mixed down to ambient conditions; *Newman et al.* [1996] and *Waugh et al.* [1997] showed that some such vortex fragments were still present in May 1993 in the Arctic. Consistent with the colder winter and later final warming in the SH, minimum high latitude temperatures at 465 K were ~6–8 K lower during AT-3 than during AT-2.

At both representative levels shown in Plate 1, AT-3 and AT-2 provided good coverage of the vortex, including observations in the vortex core. During AT-3, air was drawn up around the vortex from sufficiently low latitudes that AT-3 sampled subtropical air. During AT-2, since the ATMOS observations covered a narrower latitude band and less air was being drawn in from low latitudes, little subtropical air was sampled.

In fall there is less interhemispheric [e.g., *Manney and Zurek*, 1993] and, in both hemispheres, less interannual [e.g., *O'Neill and Pope*, 1990] variability in dynamical processes

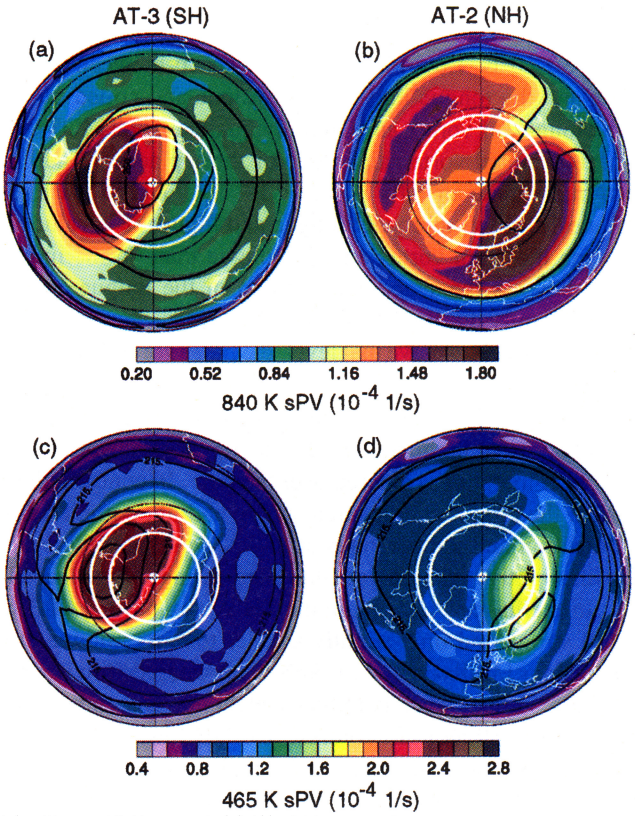


**Plate 1.** Maps of the absolute value of scaled potential vorticity (|sPV|) on the 840 K isentropic (potential temperature, θ) surface, averaged over (a) November 4-11, 1994, during AT-3 and (b) April 8-15, 1993, during AT-2, in the spring hemisphere (southern hemisphere (SH) for AT-3 and northern hemisphere (NH) for AT-2), and on the 465 K surface for (c) AT-3and (d) AT-2. Absolute value is shown since sPV decreases (to higher negative values) toward the pole in the SH. Overlaid in black are temperature contours of (a and b) 230, 240, and 250 K at 840 K and (c and d) 205, 210, and 215 K at 465 K. The thick white circles show the bounds of the latitude coverage during the AT-3 and AT-2 missions. The map projection is orthographic, with 0° longitude at the bottom in the NH maps and at the top in the SH maps, and 90°E to the right. The domain is from equator to pole, with thin dashed lines at 30° and 60° latitude.

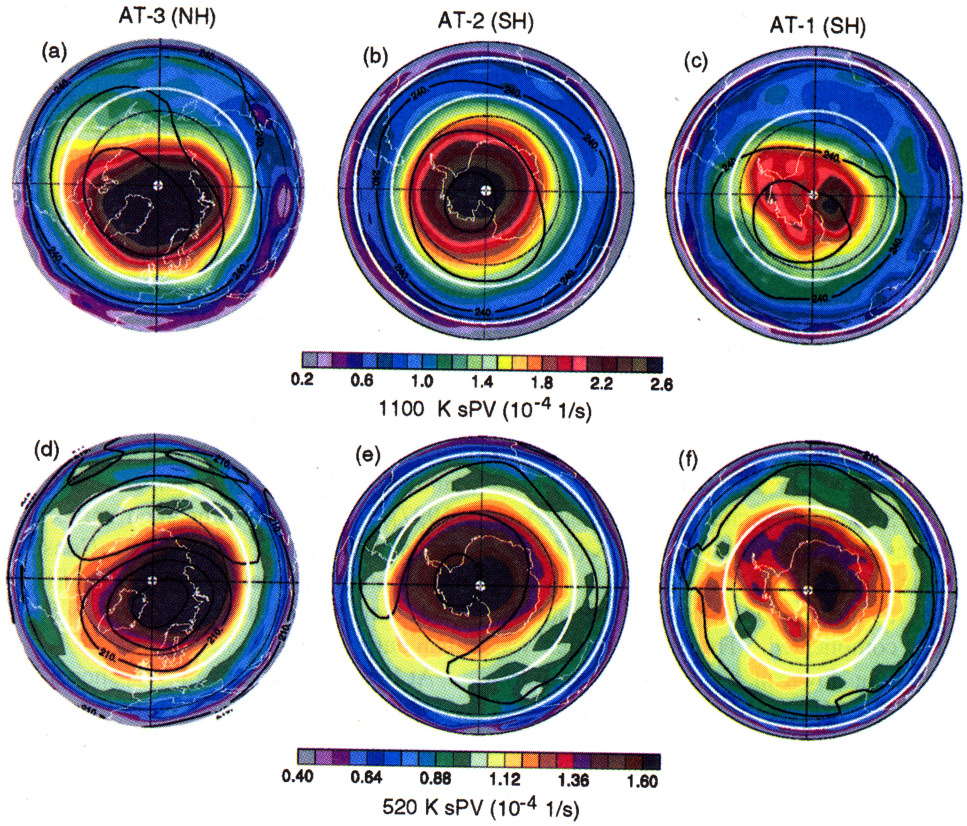


**Plate 2.** Maps of |sPV| on the (a–c) 1100 K and (d–f) 520 K isentropic surfaces, averaged over (a and d) November 4–11, 1994, during AT-3, (b and e) April 8–15, 1993, during AT-2, and (c and f) March 25–April 1, 1992, during AT-1, in the fall hemisphere (NH for AT-3, SH for AT-2 and AT-1). Overlaid in black are temperature contours of (a–c) 220, 230, and 240 K at 1100 K and (d–f) 205, 210, and 215 K at 520 K. The thick white circles show the bounds of the latitude coverage during the AT-3 (the low-latitude circle is along the edge of the plot), AT-2, and AT-1 missions. The layout is as in Plate 1, except different θ levels are shown.

than in winter or spring. In keeping with smaller interannual and interhemispheric variability, fall meteorological conditions during the three ATLAS missions (Plate 2) show differences that are consistent with the protovortex being more fully developed (stronger PV gradients, higher PV in the vortex) during each succeeding mission; observations were taken ~2 weeks later in the season in AT-2 than AT-1 and another 2 weeks later in AT-3 than in AT-2. The fall polar vortices develop from the top down [e.g., *Waugh and Randel*, 1999], as is evident in the better-defined protovortex at 1100 K than at 520 K. *Manney et al.* [1996b] showed that the protovortex was evident at levels down to ~450 K during AT-3; a significant region of strong PV gradients extends only down to ~500 K during AT-2. As seen in Plate 2f, during AT-1 there was only a very small region of enhanced PV gradients at 520 K. The temperatures also indicate more winter-like conditions during each succeeding mission, especially at 520 K, where the temperatures were dropping rapidly at this time.

The protovortices in the middle and upper stratosphere during AT-1 and AT-3 were distorted and shifted off the pole (Plate 2a and 2c). In contrast, the protovortex during AT-2 (Plate 2b) was, on average, symmetrical and pole centered. During all three missions, however, maps for individual days show that the protovortex wobbled about and tongues of air were drawn off the vortex edge. During AT-3 the vortex was preferentially shifted toward the Greenwich meridian, as is typically the case later in the Arctic winter when the "Aleutian high" has formed [e.g., *Juckes and O'Neill*, 1988], and tongues of air were pulled off near ~250°E and drawn out to ~30°N (G. L. Manney et al., ATMOS profile structure, filamentation, and transport around the 1994 Arctic protovortex, submitted to *Journal of Geophysical Research*, 1999). During AT-2 the vortex shape and position were more variable and smaller tongues of material were pulled off the edge at several locations on different days; on April 12-14, 1993, the protovortex extended towards the date line and a tongue of material drawn off the vortex edge near ~150°E was pulled out to nearly 30°N. During AT-1 the protovortex area was smaller, and, although material can be seen drawn off the edge, these events were smaller, shorter lived, and did not in general transport protovortex air to latitudes as low as in AT-2 and AT-3. The situation in the lower stratosphere during the three missions was roughly similar to that at the higher levels, except that the vortex was just beginning to develop, and thus PV gradients were still much weaker than winter values and, especially during AT-1, did not yet represent a substantial transport barrier.

Although the fall ATMOS observations extended up to only ~50° (Table 1), the variability described above enabled ATMOS to sample protovortex air during each mission. The sampling was better in AT-3 than AT-2 or AT-1; although the protovortex was stronger during AT-2 than AT-1, the sampling range was very limited (Plate 2).

Because of the variability and asymmetry of the vortex, the ATMOS observations taken in limited latitude bands cover a wide variety of meteorological conditions. By viewing these observations from a vortex-centered perspective, we can examine how the meteorological conditions shaped the detailed structure of the trace gas fields measured by ATMOS using a physically based context for comparison between the missions.

## 3. Data and Analysis

### 3.1. ATMOS Data

The horizontal coverage of the ATMOS data was summarized in Table 1 (section 2). The ATMOS version 2 data cover altitudes ranging from 12 to 80 km with a vertical resolution of 2–3 km [e.g., *Abrams et al.*, 1996b]. For each occultation the signal-to-noise ratio was optimized by the use of one of a set of six optical bandpass filters (numbered 1, 2, 3, 4, 9, and 12; some filters were not used in all missions). $N_2O$ was measured with all six filters; $CH_4$, $O_3$, and $HNO_3$ were measured in five filters; $H_2O$ was measured in four; and other trace gases were measured in three or fewer. *Gunson et al.* [1996] summarize the altitude coverage, filters used, and estimated precision for each species.

A summary of some critical features of the processing methodology and discussion of the error budget for the version 2 ATMOS data is given by *Abrams et al.* [1996b]. The experimental uncertainties vary with species, filter, and altitude. $O_3$, $N_2O$, $CH_4$, and $HNO_3$ typically have precision better than 5%; $H_2O$ and $NO_2$ typically have precision better than 10%; NO and $N_2O_5$ typically have precision better than 20%; and $ClONO_2$ and $HNO_4$ have precision worse than 20%. Data from filter 4 (filter 12) were excluded below 30 km (20 km) because of systematic biases.

At the top and bottom altitudes of the measurement range, the ATMOS version 2 data occasionally include some unphysical values that are not accompanied by large uncertainties. In order to detect and remove the worst of these, the tops and bottoms of the profiles were checked for unphysically large gradients and negative mixing ratios before gridding, and a few points from some profiles were excluded on this basis. These "quality-control" criteria were adjusted so as to exclude most of the values identified as unrealistic but to include all values that could be physically based. The number of data points excluded is small, typically 0-10 for a given species and mission.

### 3.2. Equivalent-Latitude/θ Mapping of ATMOS Data

PV and sPV from UKMO data, interpolated (bilinearly in the horizontal and linearly in log-pressure in the vertical) to the ATMOS observation locations, are provided with the version 2 ATMOS data. This sPV is used to grid the ATMOS data in EqL/θ space by taking a weighted average of all observations falling within a prescribed distance in PV and logθ of the desired grid point. As well as being weighted by distance, the values averaged at each grid point are weighted by the estimated retrieval uncertainty using the same function as for the spatial weighting, with the error half width and cutoff determined by the expected precision for each species [*Abrams et al.*, 1996b]. Various combinations of weighting parameters were tested and compared with unweighted av-

erages of binned data. The gridding is not particularly sensitive to the weighting function; a Gaussian was used in the plots shown below. The half width in θ was selected so as to make the vertical spacing ~2 km, comparable to the vertical resolution of the ATMOS data. The selection of half width in PV is more problematic and is based on striking a balance between a reasonable number of grid points in regions where PV gradients are weak (which argues for closer spacing) and not too many empty grid boxes in regions where there is good data coverage but PV gradients are very strong. This is particularly problematic during AT-3, when there were extremely strong PV gradients around the vortex in the austral lower stratosphere but extremely weak PV gradients in the austral upper stratosphere [*Manney et al.*, 1996b].

The PV half widths (ΔsPV) selected are $0.2 \times 10^{-4}$ s$^{-1}$ for AT-3 and $0.15 \times 10^{-4}$ s$^{-1}$ for AT-1 and AT-2. For $N_2O$ (a species that is measured in all six filters), these values give ~1–40 points in each occupied grid box for AT-3, ~1-30 for AT-2, and ~1-20 for AT-1. The gridding routine then uses all data within two half widths in PV and θ of the grid point in the average; however, a value is not calculated unless there is at least one observation within one half width of the grid point. The error weighting allows inclusion of any data with uncertainty less than 100%; since the error half widths are based on the expected precisions, typically 5–10% for the species shown here, the occasional data with large percentage errors are far out on the tails of the weighting functions and are given very little weight.

For derived products combining several species measured by ATMOS (e.g., $NO_y$), each species is individually gridded in PV/θ space and the species are combined after gridding. This method allows combination of species that were not measured simultaneously (i.e., in the same filters), but were measured under the same meteorological conditions, and thus provides the fullest coverage for the derived products. For calculations of $NO_y$, profiles of the species used are extrapolated above and below the measurement range as described by *Rinsland et al.* [1996a], except that $HNO_3$ is not extrapolated at the bottom and NO is not extrapolated at the top. Thus $NO_y$ is calculated only where ATMOS observed $HNO_3$ in the lower stratosphere (where it constitutes the bulk of $NO_y$ ) and where ATMOS observed NO in the upper stratosphere.

After gridding in PV/θ space, EqL is calculated for each PV grid point value and the fields are interpolated linearly to a uniform EqL grid. The interpolation routine is restricted from filling across large gaps; thus the coverage in the plots shown below is representative of the actual coverage of the ATMOS observations.

### 3.3. Parcel History Calculations

We use back trajectory calculations to examine the recent history of air at the locations of the ATMOS observations. The trajectory code is described by *Manney et al.* [1994c]; it is in isentropic coordinates and includes a calculation of diabatic descent to obtain vertical velocities in that coordinate system. The UKMO horizontal winds are used, and UKMO temperatures are used in the radiation calculation to estimate vertical velocities.

The initial parcel positions are determined in a manner similar to that described by *Manney et al.* [1998]. At the location (latitude and longitude) of each ATMOS observation, a column of parcels is initialized on 100 isentropic surfaces equally spaced in logθ between 380 and 2000 K (this is the same as the vertical range of the EqL/θ space plots of ATMOS data). On each surface, 121 parcels are initialized in a 1° by 1° box centered at the ATMOS measurement location, giving 12,100 total parcels for each ATMOS profile. Back trajectory calculations are run for 32 days, each started from the time (closest 1/2 hour, the trajectory time step) of the corresponding ATMOS observation.

For the approximately monthlong duration of the runs, the positions of individual parcels are, of course, uncertain, because of accumulated errors from a number of sources, one of the largest being inaccuracies in the advecting winds [e.g., *Morris et al.*, 1995]. However, much useful information can be obtained from three-dimensional trajectory calculations of this length, provided a reasonably large number of parcels are averaged. For example, *Manney et al.* [1997, and references therein] successfully computed vortex-averaged trace gas values using 30- to 40-day trajectory-based transport calculations. Trajectory calculations of several months' duration have frequently been used to examine general features of air motion [e.g., *Fisher et al.*, 1993; *Manney et al.*, 1994c]. A very large number of parcels is used here (~2.1 million for AT-3, 1.1 million for AT-2, and 1.0 million for AT-1) to facilitate averaging over various domains.

Results from the trajectory calculations are displayed by mapping the historical characteristics of the parcels into EqL/θ space in the same manner as for the ATMOS data. That is, the positions of the parcels (e.g., latitude, Δθ, sPV) at the end of the back trajectory run, or data (e.g., idealized trace gas fields) interpolated to those positions, are taken as the field to be gridded, with the gridding coordinates being the initial positions (PV, θ) at the ATMOS observation locations. This produces a map of the characteristics 32 days earlier of the air sampled by ATMOS. If the same PV/θ grid is used as for the ATMOS data, there are ~50 to several thousand parcels in each grid box, providing reasonable statistics for averaging. The gridding procedure is the same as described above for the ATMOS data, except that no weighting for uncertainty is used. Because there are many parcels in each grid box, the scatter in values within a box gives information on the homogeneity of the historical characteristics of air that ended up in a certain region sampled by ATMOS.

Besides examining vertical and horizontal motion and PV changes over the period, we have produced idealized transport calculations over the period for $N_2O$, $CH_4$, and $H_2O$ by using idealized tracers derived from UARS Microwave Limb Sounder (MLS) or Cryogenic Limb Array Etalon Spectrometer (CLAES) data (section 3.4) interpolated to the final parcel positions as the field to be gridded. This is an application of the reverse-trajectory procedure developed and described in detail by *Sutton et al.* [1994]. It assumes that trace gases are passively transported for the duration of the

calculations, a good assumption for $N_2O$, $CH_4$, and $H_2O$ during spring/fall for the duration of the trajectory calculations and the range of levels studied here [e.g., *Brasseur and Solomon*, 1986]; although the lifetime of $N_2O$ is shorter above ~40 km, its mixing ratio is so low at these levels that small chemical changes would not significantly affect our transport calculations. The UARS-based fields used for tracer initialization are very smooth, and we expect only large-scale qualitative agreement between these fields and ATMOS data; nevertheless, the qualitative changes in tracers resulting from these transport calculations are useful for comparison with the ATMOS observations.

### 3.4. Ancillary Data

We use data from the UARS CLAES and MLS instruments to produce idealized tracer initialization fields and to illuminate certain aspects of the flow during the ATLAS missions. During all three ATLAS missions the latitude coverage of the UARS observations we use was ~80°S to 30°N. Both CLAES and MLS were fully operational during AT-1 and AT-2; AT-3 occurred after CLAES had depleted its cryogen and the radiometer that measured $H_2O$ on MLS had failed. MLS did, however, measure $O_3$, $HNO_3$, and ClO during most (November 5 through 11, 1994) of AT-3.

For model initialization we have constructed a set of idealized tracer fields in EqL/θ space from CLAES $N_2O$ and $CH_4$ and MLS $H_2O$. Since UARS switches 10 times a year between viewing high northern and high southern latitudes (yaws), in order to get global fields, we average (in EqL/θ space) the data from 3 days with complete coverage on either side of the yaw day. Data from late April 1992 through early April 1993 are used to produce 10 such files for each species (one for each "UARS month"), each of which is assigned to the day of year in the middle of the averaging period. To reconstruct a field for a particular day, the PV for that day is used with an EqL/θ field of the tracer that is linearly interpolated in time between the nominal dates of the two neighboring standard EqL/θ fields. The data used to produce the files for this "climatology" are version 8 CLAES $N_2O$, version 7 CLAES $CH_4$, and MLS $H_2O$ from the prototype nonlinear retrievals described by *Pumphrey* [1998]. Version 7 CLAES $N_2O$ and $CH_4$ validation is discussed by *Roche et al.* [1996]; version 8 $CH_4$ is not used because it showed an even stronger high bias than version 7 when compared to correlative data.

We also show some MLS $O_3$ data taken during AT-3; these are preliminary version 5 data. The MLS version 3 $O_3$ data validation is discussed by *Froidevaux et al.* [1996]; some version 3/version 4 differences are noted by *Manney et al.* [1996a]. Version 5 data have higher vertical resolution than the previous versions (six surfaces per decade in pressure as opposed to three). Previous biases (~1 ppmv) in the MLS lower stratospheric $O_3$ data, as compared to SAGE II and other correlative sources, have been significantly reduced in the version 5 data; differences between version 4 and 5 in the middle and upper stratosphere are small (N. J. Livesey et al., in preparation, 1999).

## 4. Results

### 4.1. ATMOS Trace Gas Fields

Plate 3 shows EqL/θ space plots of ATMOS $N_2O$ and $CH_4$ observations from the ATLAS missions. The overlaid |sPV| contours indicate the position and strength of the polar vortex. $N_2O$ and $CH_4$ are both long lived in the stratosphere and are thus good tracers of air motions.

The mapping of AT-3 and AT-2 sunrise observations, in the Antarctic and Arctic spring vortices, respectively, demonstrates dramatically how fully the ambient conditions can be covered with observations taken in a very narrow latitude band (approximately 8° and 6° wide for AT-3 and AT-2, respectively). Since subtropical air was drawn into the region of ATMOS observations throughout the AT-3 mission at most levels shown (Plate 2 and section 2), AT-3 sampled subtropical conditions everywhere except below ~450 K, where motions are dominated by smaller scales and large tongues of air are not commonly transported as far from their origins [e.g., *Pierce et al.*, 1994]. The variability during AT-2 was large enough to give good coverage of midlatitude conditions through most of the stratosphere. In fall the protovortex was sufficiently variable that the measurements typically reached ~60° EqL, inside the protovortex edge.

Several previously noted features of tracer transport in relation to the polar vortex are apparent in the ATMOS $N_2O$ and $CH_4$ fields. The effects of net descent through the winter [*Abrams et al.*, 1996a, c] are apparent in Plate 3, with much lower vortex than extravortex values of the tracers at all levels below about 1000 K (where air is still relatively confined within the vortex) in the spring vortices. $CH_4$ values typical of the lower mesosphere ($\lesssim$0.3 ppmv) were seen at levels from ~650 to 840 K (~25–30 km) during AT-3, and values typical of the upper stratosphere were seen at levels from ~500 to 650 K during AT-2. The packing of tracer contours into the lower stratospheric vortex (i.e., extremely large vertical tracer gradients in the vortex interior) results from the pattern of descent, which is strongest in the upper stratosphere and decreases by more than an order of magnitude from the upper to the lower stratosphere [e.g., *Fisher et al.*, 1993; *Manney et al.*, 1994c]. Substantial horizontal tracer gradients are apparent across the vortex edge even at the lowest levels shown (down to 380 K in the SH). The apparent lack of contrast between AT-3 vortex and extravortex values in the lower stratosphere noted by *Abrams et al.* [1996a] was due in part to the saturation of their color palette and the packing of contours in the lower stratospheric vortex.

A feature that was not apparent in previous studies is the downward excursion of tracer contours along the vortex edge in the lower stratosphere (at the location of strongest sPV gradients), which is seen in both NH and SH spring. This observation suggests that there was greater descent along the vortex edge than in its center. This pattern is consistent with the calculations of *Manney et al.* [1994c], *Pierce et al.* [1994], and *Eluszkiewicz et al.* [1995], which showed largest descent rates in the lower stratosphere along the vortex edge

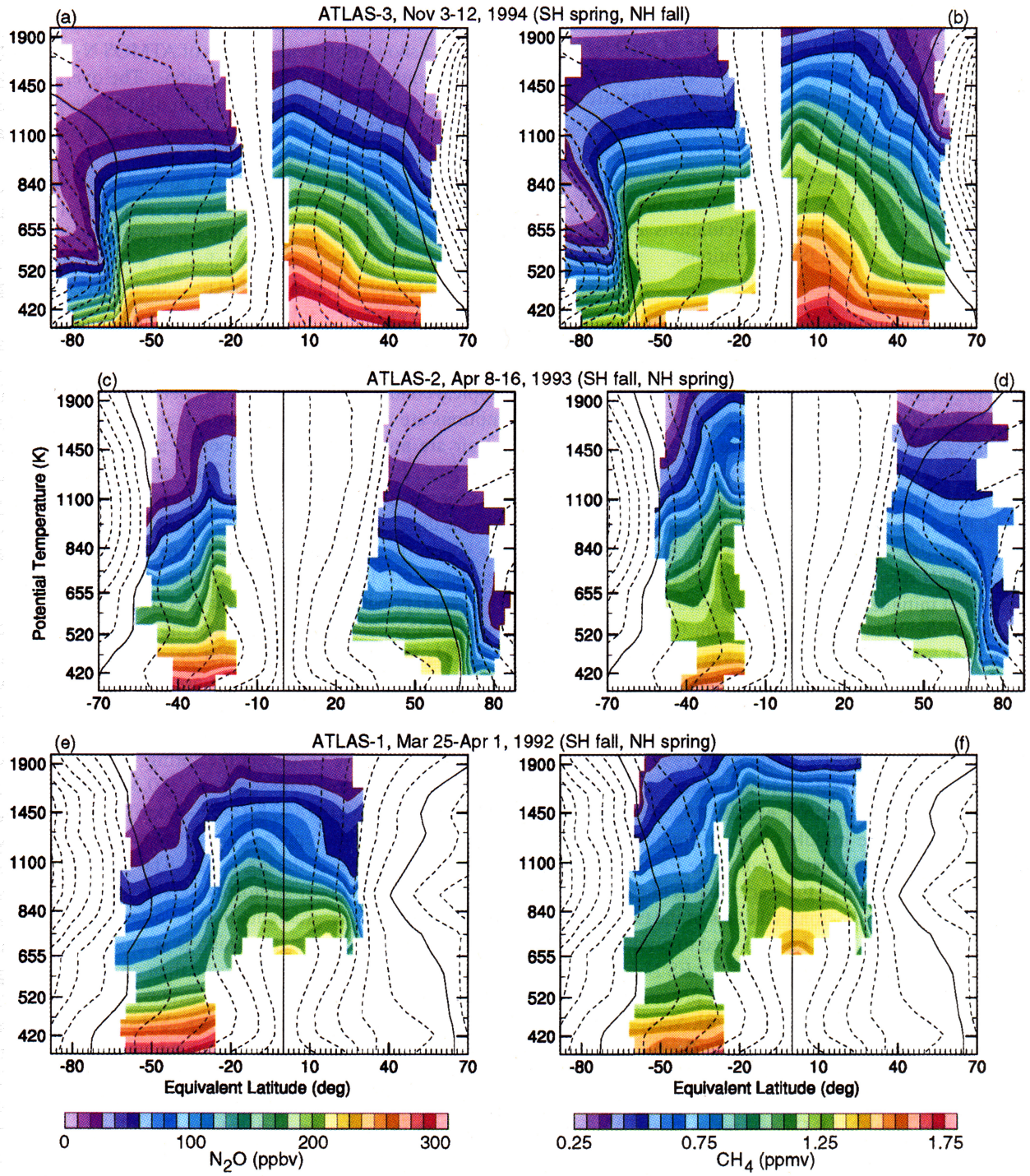


**Plate 3.** Equivalent latitude (EqL)/θ space fields of (left) ATMOS $N_2O$ and (right) $CH_4$ from (a and b) AT-3, (c and d) AT-2, and (e and f) AT-1. The vertical range is from 380 to 2000 K. AT-3 and AT-1 fields are shown from 88°S to 70°N; AT-2 fields are shown from 70°S to 88°N. The thin black lines are contours of |sPV|, averaged for AT-3 over November 4–11, 1994, for AT-2 over April 8–15, 1993, and for AT-1 over March 25–April 1, 1992 (the same days shown in Plates 1 and 2; days at the beginning and end of the ATLAS missions with only one or two ATMOS observations are excluded); the contour interval is $0.2 \times 10^{-4}$ $s^{-1}$, with the $1.2 \times 10^{-4}$ $s^{-1}$ contour (typically in the vortex edge region) represented by a solid line and the rest denoted by dashed lines; the smallest contour is $0.2 \times 10^{-4}$ $s^{-1}$ on either side of the vertical line representing 0° EqL, with values increasing toward the poles. Note that for AT-2 and AT-1 the sPV contour interval shown here is not the same as the interval used for gridding (section 3.2).

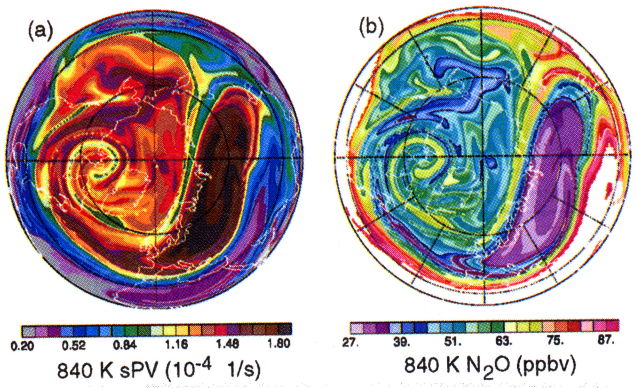


**Plate 4.** High-resolution NH maps of (a) sPV and (b) reconstructed $N_2O$ on the 840 K isentropic surface, on April 16, 1993, the last day of AT-2. The maps are constructed using reverse-trajectory calculations (section 3.3). The map projection is orthographic, with 0° longitude at the bottom and 90°E to the right. The domain is from equator to pole, with thin dashed lines at 30° and 60°N.

throughout the winter in the SH and during late winter/spring in the NH. This pattern is also reflected in $N_2O/CH_4$ correlations for AT-3, which show a larger difference between the vortex edge and midlatitude correlations than between the vortex interior and midlatitude correlations (H. A. Michelsen et al., Maintenance of high $HCl/Cl_y$ and $NO_x/NO_y$ in the Antarctic vortex: A chemical signature of confinement during spring, submitted to *Journal of Geophysical Research*, 1999) (hereafter referred to as submitted manuscript, 1999).

Above ~1100 K in the SH during AT-3 and ~800 K in the NH during AT-2, strong tracer gradients are no longer apparent. The extremely large tongue of vortex material pulled out into midlatitudes during AT-2 between ~700 and 1100 K resulted in an increase in the area enclosed by PV contours near the vortex edge, while the area enclosed by contours in the vortex interior shrank (e.g., Plate 2). As noted in section 2, this large tongue of material is coiled up with some low-latitude air in the anticyclone at latitudes sampled by ATMOS. Plate 4 shows 840 K maps of high-resolution sPV from a reverse-trajectory calculation (section 3.3) and high-resolution $N_2O$ reconstructed from this sPV field and the ATMOS EqL/θ space field shown in Plate 3c. The tongue of air that was pulled off the vortex underwent considerable mixing with low-latitude air pulled in around the vortex, and PV gradients in this region are much weaker than those at the same sPV values along the vortex edge. Thus the sPV gradients seen in Plates 3c and 3d near 50° EqL are considerably weaker than those around the vortex edge, and the EqL/θ plot does not clearly indicate the presence of the relatively strong and confined vortex remnant that still exists at these levels. Above ~1100 K the vortex has dissipated and the tracer values are well-mixed combinations of former vortex and extravortex air.

As seen in Plates 3a and 3b, the region of minimum tracer mixing ratios in the vortex during AT-3 showed low values confined closer to the pole with increasing altitude, coinciding approximately with the decrease in the area enclosed by strong PV gradients. This decrease in area indicates that the vortex was severely eroded and strong mixing was taking place: low vortex tracer values have been mixed with high extravortex values, resulting in the higher values at high latitudes at levels where the vortex was breaking down. Since $N_2O$ and $CH_4$ have different vertical gradients, confined descent within the vortex results in different horizontal gradients along the vortex edge. This, in turn, results in dissimilar contour shapes for the two tracers in the vortex and along its edge, as quasi-isentropic mixing across the vortex edge affects them differently [e.g., *Strahan et al.*, 1996]. Thus the regions near the lower stratospheric vortex where the $N_2O$ and $CH_4$ contour shapes differ markedly (e.g., between ~600 and 800 K in the SH during AT-3) are regions of enhanced mixing of vortex and extravortex air. We will return to this point in section 4.2.

More subtle variations in tracer morphology indicate differing dynamical conditions in the fall hemispheres during the three missions. In each succeeding mission the contours are overall tilted more steeply down at high EqL, indicating the effects of more unmixed descent as the vortex develops. The increase in unmixed descent results from both an increase in the diabatic descent rates and, more importantly, a stronger transport barrier along the protovortex edge, so that the effects of descent are not diluted by mixing with air that has not experienced strong descent. Both effects are consistent with greater vortex strength (section 2) in each succeeding mission. A distinct difference in the strength of the subtropical horizontal tracer gradients in the fall hemisphere, especially in the upper stratosphere, was seen between AT-1 and AT-3 (near 20 to 30° EqL); although AT-2 observations did not extend as far into the tropics, the tracer gradients during this mission appeared to be similar to those during AT-1; these patterns are consistent with those seen in zonal means of Halogen Occultation Experiment (HALOE) observations for similar time periods [*Ruth et al.*, 1997], and they likely result from the interplay between the seasonal cycle, the semiannual oscillation, and the quasi-biennial oscillation [e.g., *Ruth et al.*, 1997; *Randel et al.*, 1998].

ATMOS measured several other long-lived species, including HF, F11, F12, and $SF_6$ [*Gunson et al.*, 1996], as well as CO, which is sufficiently long lived in some regions to use as a tracer of air motion [*Allen et al.*, 1999]. Since these species had either limited vertical coverage or were measured in only one or two filters, EqL/θ maps (not shown) of them are less complete. However, during AT-3 there was enough coverage to indicate that these tracer observations showed a signature of unmixed descent within the vortex, and those with observations near the lower stratospheric vortex edge showed the downward excursion of contours indicative of enhanced descent.

Plate 5 shows similar plots of $H_2O$ and $HNO_3$ observed by ATMOS. $H_2O$ is a long-lived tracer in most of the extratropical stratosphere, with the exception of the Antarctic lower stratospheric vortex, where sedimentation of polar strato-

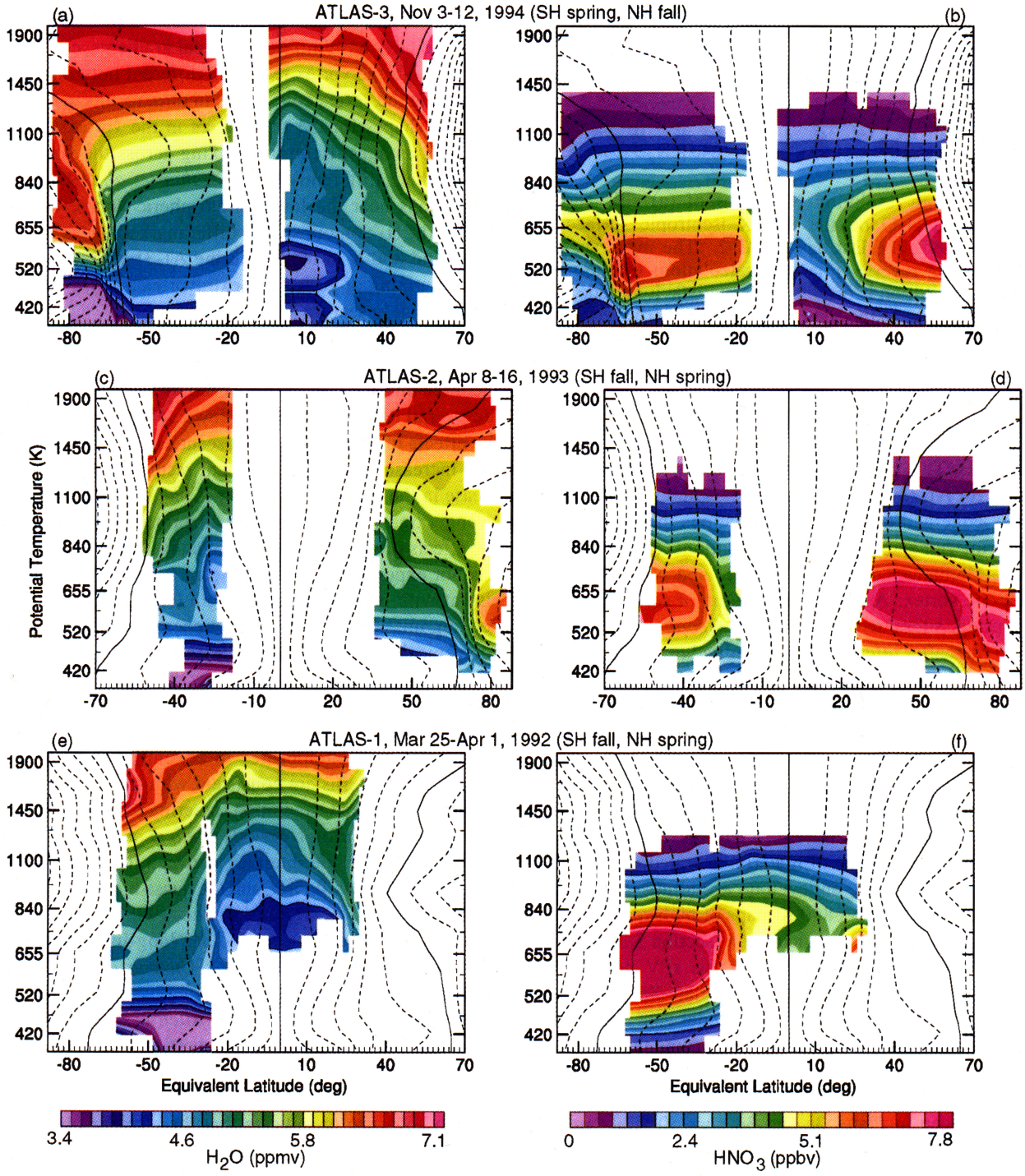


**Plate 5.** Same as Plate 3, but for EqL/θ space fields of ATMOS (left) $H_2O$ and (right) $HNO_3$.

spheric clouds (PSCs) results in severe dehydration. $HNO_3$ builds up via chemical processes in the winter polar vortex [e.g., *Austin et al.*, 1986], with maximum mixing ratios near 25 km, and builds up in the lower stratospheric vortex via descent of these high values and production by heterogeneous chemical reactions linked to PSCs [*Santee et al.*, 1999, and references therein]; in the Antarctic, PSCs are prevalent for much of the winter and sedimentation also leads to strong denitrification. Several studies have suggested that small amounts of dehydration and denitrification may occur in the Arctic vortex during especially cold winters [e.g., *Fahey et al.*, 1990b; *Vömel et al.*, 1997; *Hintsa et al.*, 1998].

The features described above in $N_2O$ and $CH_4$ are also apparent in $H_2O$, including the signature of descent in the spring polar vortices during AT-2 and AT-3, evidence of mixing at levels where the vortex was decaying, and a successively steeper downward slope of the $H_2O$ contours in the fall hemisphere in each succeeding mission. Dehydration is apparent in the SH vortex up to at least ~500 K, as shown by *Rinsland et al.* [1996a]; the highest dehydrated altitude cannot be deduced from this figure since descent of higher $H_2O$ and mixing in of lower extravortex $H_2O$ (above ~500 K) must be considered. Although the interpretation is complicated by the dehydration, a downward tilt in the $H_2O$ contours along the vortex edge in the lower stratosphere suggests stronger descent there than in the vortex core. This pattern is not apparent in the NH during AT-2, as it was in other tracers. The lack of such a feature in $H_2O$ could reflect a sampling or data quality deficiency, or may indicate a small amount of dehydration, which has previously been suggested to have occurred in the 1992-1993 Arctic winter [*Michelsen et al.*, 1999].

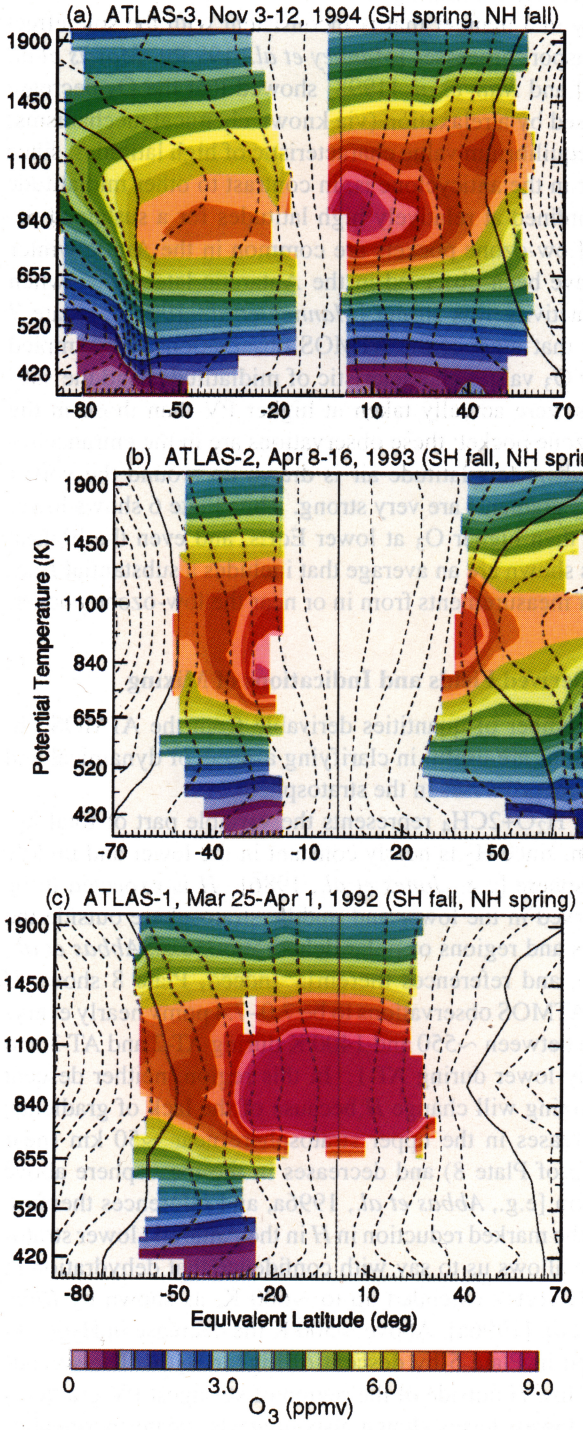


**Plate 6.** Same as Plate 3, but for EqL/θ space fields of ATMOS $O_3$.

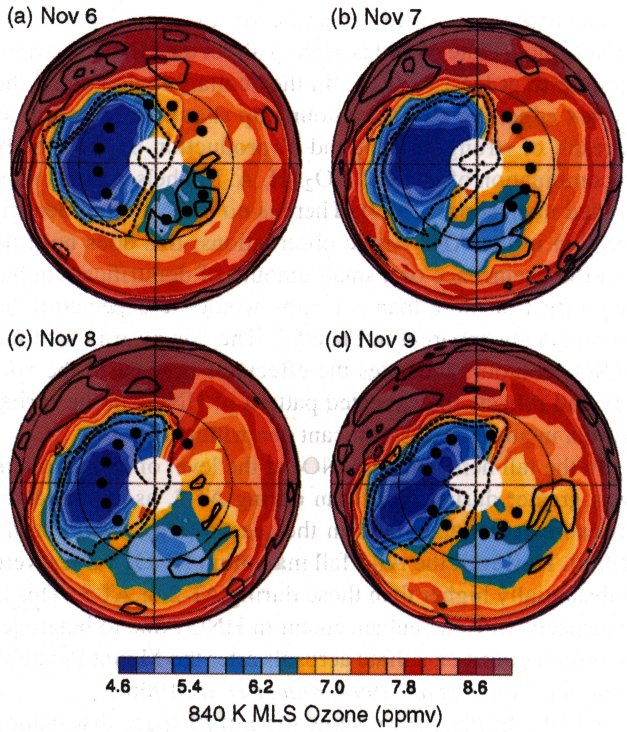


**Plate 7.** Maps of Microwave Limb Sounder (MLS) $O_3$ in the SH on the 840 K isentropic surface during the AT-3 mission on (a) November 6, (b) November 7, (c) November 8, and (d) November 9. Contours of |sPV| are overlaid in black; 1.2 and 1.4 × $10^{-4}$ $s^{-1}$ contours are dashed, while 0.6 and 0.8 × $10^{-4}$ $s^{-1}$ contours are solid. The black dots show the locations of ATMOS observations on each day. The map projection is orthographic, with 0° longitude at the top and 90°E to the right. The domain is from equator to pole, with thin dashed lines at 30° and 60°S.

Denitrification in the Antarctic vortex is apparent in the $HNO_3$ plot (Plate 5) and is seen to affect the $HNO_3$ distribution up to at least ~600 K. In the "collar" region along the vortex edge, the $HNO_3$ contours dip sharply downward, as a result of strong descent and of production by three-body recombination of OH and $NO_2$ (H. A. Michelsen et al., submitted manuscript, 1999). There is no indication of denitrification in the AT-2 Arctic observations; this does not rule out the occurrence of a small amount of denitrification, but any effect of more than ~1 ppbv would be expected to be immediately apparent in Plate 5d. The downward tilt of the $HNO_3$ contours indicates the effects of descent in the vortex and reflects the expected pattern of $HNO_3$ in the spring vortex in absence of significant denitrification.

In the fall hemisphere, $HNO_3$ at the level of its maximum was greater during AT-3 than during AT-2, as expected for measurements taken later in the season [e.g., *Austin et al.*, 1986]. However, the AT-1 fall maximum $HNO_3$ values were substantially higher than those during AT-2 or AT-3. This is consistent with the enhancement in $HNO_3$ due to heterogeneous reactions on sulfate aerosols after the Mount Pinatubo eruption [*Koike et al.*, 1994; *Kumer et al.*, 1996].

Finally, in Plate 6 we show the EqL/θ space distribution of $O_3$ observed by ATMOS during the ATLAS missions. As expected, there is widespread $O_3$ depletion in the Antarctic lower stratospheric vortex during AT-3. In the absence of chemical depletion in the lower stratosphere, $O_3$ mixing ratios are substantially higher inside than outside the vortex below ~600 K [e.g., *Manney et al.*, 1995a, and references therein]; thus the comparable values seen inside and outside the Arctic lower stratospheric vortex during AT-2 are indicative of chemical $O_3$ loss, consistent with previous studies of that winter [*Manney et al.*, 1995c; *Michelsen et al.*, 1998b, and references therein]. Since descent masks chemical $O_3$ loss in the vortex, $O_3$ depletion occurred up to higher altitudes than is immediately apparent; previous studies of the 1992-1993 winter indicate some $O_3$ depletion up to ~550 K [e.g., *Manney et al.*, 1995c, and references therein].

The main source of $O_3$ is in the tropical middle stratosphere, with mixing ratios exceeding 10 ppmv in the equatorial regions near 30–35 km [e.g., *Brasseur and Solomon*, 1986], high mixing ratios extending into midlatitudes in the middle stratosphere as air is transported poleward, and very strong gradients across the vortex edge as that air encounters a barrier to further poleward transport [e.g., *Manney et al.*, 1995a, and references therein]. The poleward and upward tilt of the level of peak mixing ratios seen in Plate 6 is characteristic of the early winter $O_3$ distribution and has been attributed to a combination of photochemical and vertical transport processes [e.g., *Manney et al.*, 1995a, and references therein]; in monthly mean values shown by *Randel and Wu* [1995], this pattern is not well developed until November (May) in the NH (SH), suggesting that the stronger pattern during AT-3 is due to the later observation time.

Given the expected distribution and sources of $O_3$, the ATMOS values during AT-3 in SH middle EqLs look decidedly peculiar and are, in fact, in disagreement with values observed by UARS MLS during this period. The reason for this discrepancy provides a note of caution in interpreting EqL/θ space plots of chemically active species. Examination of maps of MLS $O_3$ in the SH middle stratosphere during AT-3 (Plate 7) shows that many of the ATMOS observations at low EqL (i.e., low PV, solid contours) were taken in or near a "low-ozone pocket" [*Manney et al.*, 1995b]. Low-ozone pockets form in the middle stratosphere near the level of the $O_3$ maximum when low-latitude, high-$O_3$ air is drawn poleward and confined for a number of days in the anticyclone; $O_3$ mixing ratios in this confined air decrease rapidly in a manner that is inconsistent with the sole effect of transport processes [*Manney et al.*, 1995b]. *Morris et al.* [1998] and *Nair et al.* [1998] showed that the $O_3$ decrease is caused by a relaxation (via known chemical mechanisms) to an equilibrium value characteristic of high latitudes, since the air in the anticyclone is, in contrast to other midlatitude air, confined at relatively high latitudes for a sustained period. Low-ozone pockets are common in the Arctic winter and have been observed in the Antarctic late winter when wave activity was strong [*Manney et al.*, 1995b]. Plate 7 shows that most of the ATMOS observations that sampled higher $O_3$ values characteristic of midlatitudes and the subtropics were actually taken at higher PV than those in the low-ozone pocket; these observations are in the entrance region where low-latitude air is drawn up around the vortex and $O_3$ gradients are very strong. Thus Plate 6 shows lower rather than higher $O_3$ at lower EqLs, and even the highest values shown are an average that includes a substantial fraction of measurements from in or near the low-ozone pocket.

### 4.2. Derived Fields and Indications of Mixing

A number of quantities derivable from the ATMOS observations are useful in clarifying aspects of dynamical and chemical processes in the stratosphere.

$H = H_2O+2CH_4$ represents the variable part of total hydrogen, since $H_2$ is nearly constant in the lower and middle stratosphere [e.g., *Jones et al.*, 1986]. $H$ is expected to be conserved in the lower and middle stratosphere outside the tropics and regions of polar dehydration [e.g., *Abbas et al.*, 1996b, and references therein]. Indeed, Plate 8 shows $H$ from ATMOS observations to be 7.0–7.4 ppmv nearly everywhere between ~550 and 1400 K during AT-2 and AT-3 and slightly lower during AT-1. In this region, neither descent nor mixing will change $H$ because of the lack of gradients; $H$ increases in the upper stratosphere near ~50 km (near the top of Plate 8) and decreases in the mesosphere above ~60 km [e.g., *Abbas et al.*, 1996a, and references therein]. Thus the marked reduction in $H$ in the Antarctic lower stratosphere allows us to say with confidence that dehydration in the SH vortex extended up to ~600 K, as shown by *Rinsland et al.* [1996a]. Above ~500 K the decrease in $H_2O$ was masked in Plate 5 by descent of higher $H_2O$. The spreading of low $H$ outside of the region of strongest PV gradients at the lowest levels shown also suggests greater permeability of the vortex below ~420 K, consistent with theoretical calculations [e.g., *Manney et al.*, 1994c].

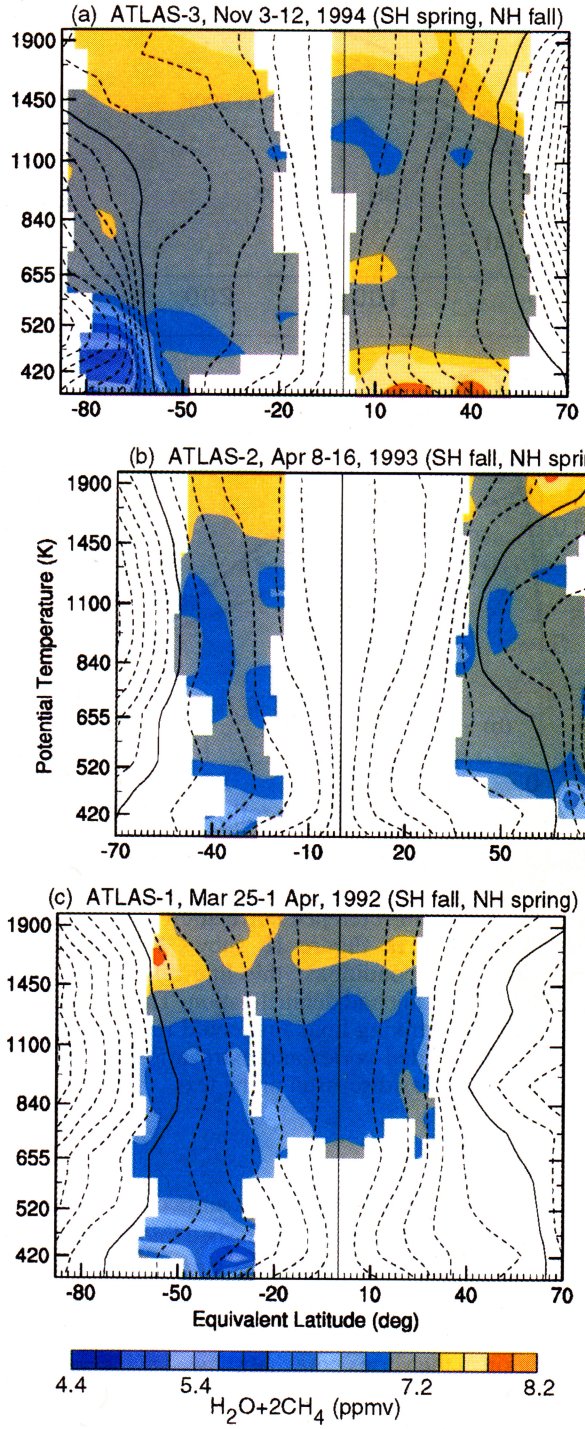


**Plate 8.** Same as Plate 3, but for EqL/θ space fields of ATMOS $H_2O+2CH_4$.

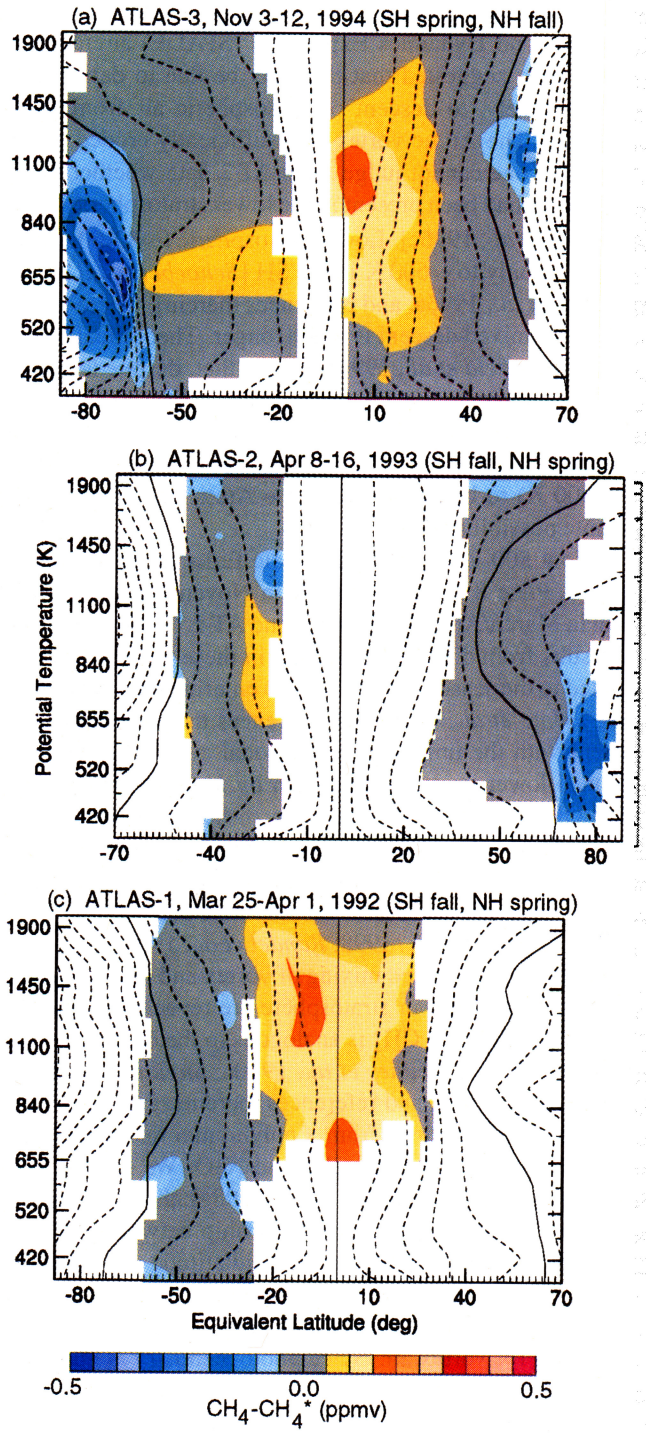


**Plate 9.** Same as Plate 3, but for EqL/θ space fields of ATMOS $CH_4$-$CH_4^*$ (see text).

A decrease of ~0.6–0.8 ppmv in $H$ was seen in the Arctic vortex during AT-2 (Plate 8b) below ~500 K, consistent with values calculated for vortex averages by *Michelsen et al.* [1999]. *Michelsen et al.* [1999] showed that this decrease was consistent with observations made in vortex fragments several weeks later during the Stratospheric Photochemistry, Aerosols and Dynamics Expedition (SPADE) aircraft mission. They suggested that this may be due to dehydration or, alternately, to descent of mesospheric air from above ~60 km. The Arctic vortex was sufficiently eroded during AT-2 that one cannot judge from AT-2 data whether mesospheric air had been present in the lower stratospheric vortex [*Abrams et al.*, 1996c]. Lower mesospheric (~50-60 km) air descends only to ~600 K in the SH [*Schoeberl et al.*, 1995; *Abrams et al.*, 1996a, and references therein], where the period of unmixed descent is much longer. Theoretical studies [e.g., *Rosenfield et al.*, 1994] suggest that, despite larger descent rates than in the SH, upper stratospheric air (~50 km) descends only to ~23-25 km (~500-550 K) over the NH winter. Thus descent of mesospheric air from above 60 km (~2800 K) to below 500 K in the Arctic seems, at best, a remote possibility.

Below 500 K in low and middle EqLs in the fall hemisphere, Plate 8 shows higher $H$ in November during AT-3 than in March/April during AT-2 and AT-1. The difference in $H$ results from differences in $H_2O$ in these regions (Plate 5) related to the seasonal cycle in $H_2O$ entering the stratosphere [e.g., *Mote et al.*, 1996, and references therein] and is consistent with the timing of the seasonal cycle in $H_2O$ in the tropical lower stratosphere shown by *Mote et al.* [1996] in HALOE and SAGE II data. The overall increase in $H_2O$ (Plate 5) and $H$ (Plate 8) throughout the stratosphere between AT-1 and AT-3 (~2.5 years) is consistent with recent trend studies [*Oltmans and Hofmann*, 1995; *Nedoluha et al.*, 1998a, b; *Evans et al.*, 1998; *Randel et al.*, 1999].

Regions of enhanced mixing of vortex and extravortex air in the middle to lower stratosphere are revealed in maps of $CH_4$-$CH_4^*$ (Plate 9). $CH_4^*$ is analogous to the commonly calculated $NO_y^*$ [e.g., *Fahey et al.*, 1990a; *Sugita et al.*, 1998; *Kondo et al.*, 1999, and references therein]; that is, it is the expected $CH_4$ obtained from a polynomial relationship appropriate for fall between $CH_4$ and $N_2O$. We use the relationship given by *Michelsen et al.* [1998a]; they showed that because there is a nonlinear relationship between $N_2O$ and $CH_4$ for $N_2O \lesssim 200$ ppbv for fall midlatitude and protovortex air, the mixing of air that had descended in the vortex with extravortex air produced a change in the $CH_4/N_2O$ relationship for vortex air. Since photochemistry is not likely to significantly modify vortex abundances of either $CH_4$ or $N_2O$ over the winter, the changes in the $CH_4/N_2O$ correlation were attributed to mixing of vortex (originally from high altitudes) and extravortex (from low altitudes) air. Figure 1a shows schematically examples of changes in the $CH_4/N_2O$ correlation anticipated to result from mixing at various levels. Plate 9 shows the differences between $CH_4^*$ (derived from the thick solid curve in Figure 1a) and the observed $CH_4$. Deviations from zero indicate regions where mixing of

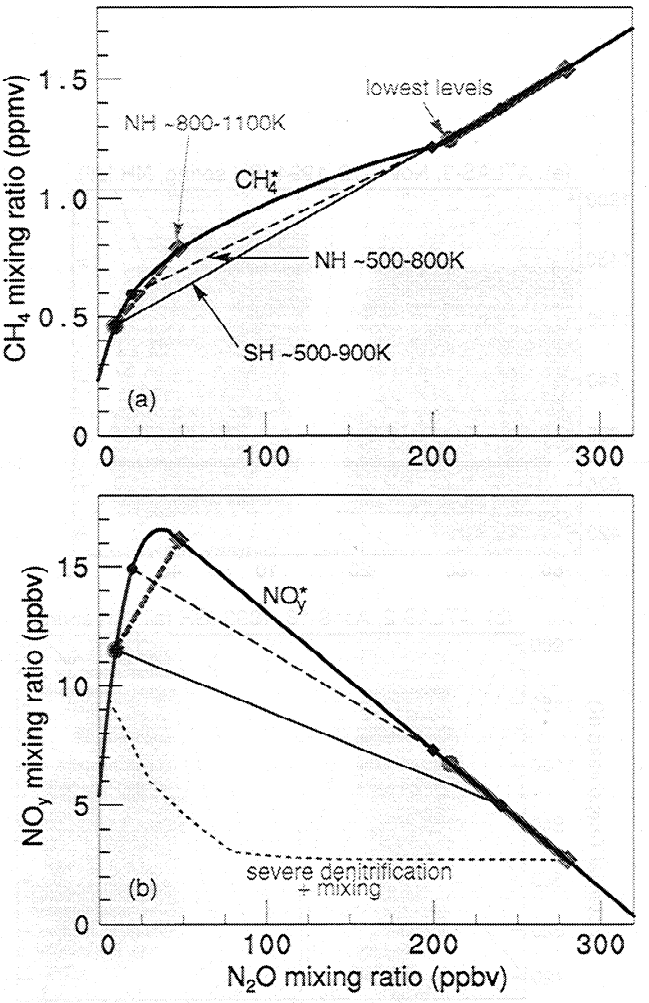


**Figure 1.** Schematic showing possible changes in (a) $CH_4$ and (b) $NO_y$ correlation curves due to mixing. The thick black curve is the fall reference correlation with $N_2O$. The stippled dotted line in Figure 1b shows $NO_y$ typical of severely denitrified conditions; this line reflects the combined effects of mixing and denitrification. The other curves show examples of mixing lines that could result from mixing between descended-vortex and extravortex air in spring at various altitudes, as discussed in the text.

descended vortex air with extravortex air occurred, schematically indicated by the thin solid or dashed lines in Figure 1a. In the SH during AT-3 (Plate 9a), the strongest signature of mixing was along the edge of the vortex at levels where it was strongly eroded, ~600–900 K. Below ~700 K there was a small region in the vortex core that showed evidence of less mixing, consistent with previous studies, which found that mixing with extravortex air took place along the Antarctic vortex edge but not deep in the interior [e.g., *Bowman*, 1993; *Manney et al.*, 1994c]. Below 420 K (Figure 1a, solid stippled line), mixing would not affect the $CH_4/N_2O$ relationship since $N_2O$ values were sufficiently high both inside and outside the vortex that the two initial air masses spanned a linear part of the correlation curve.

In the Arctic during AT-2 (Plate 9b), the air in the vor-

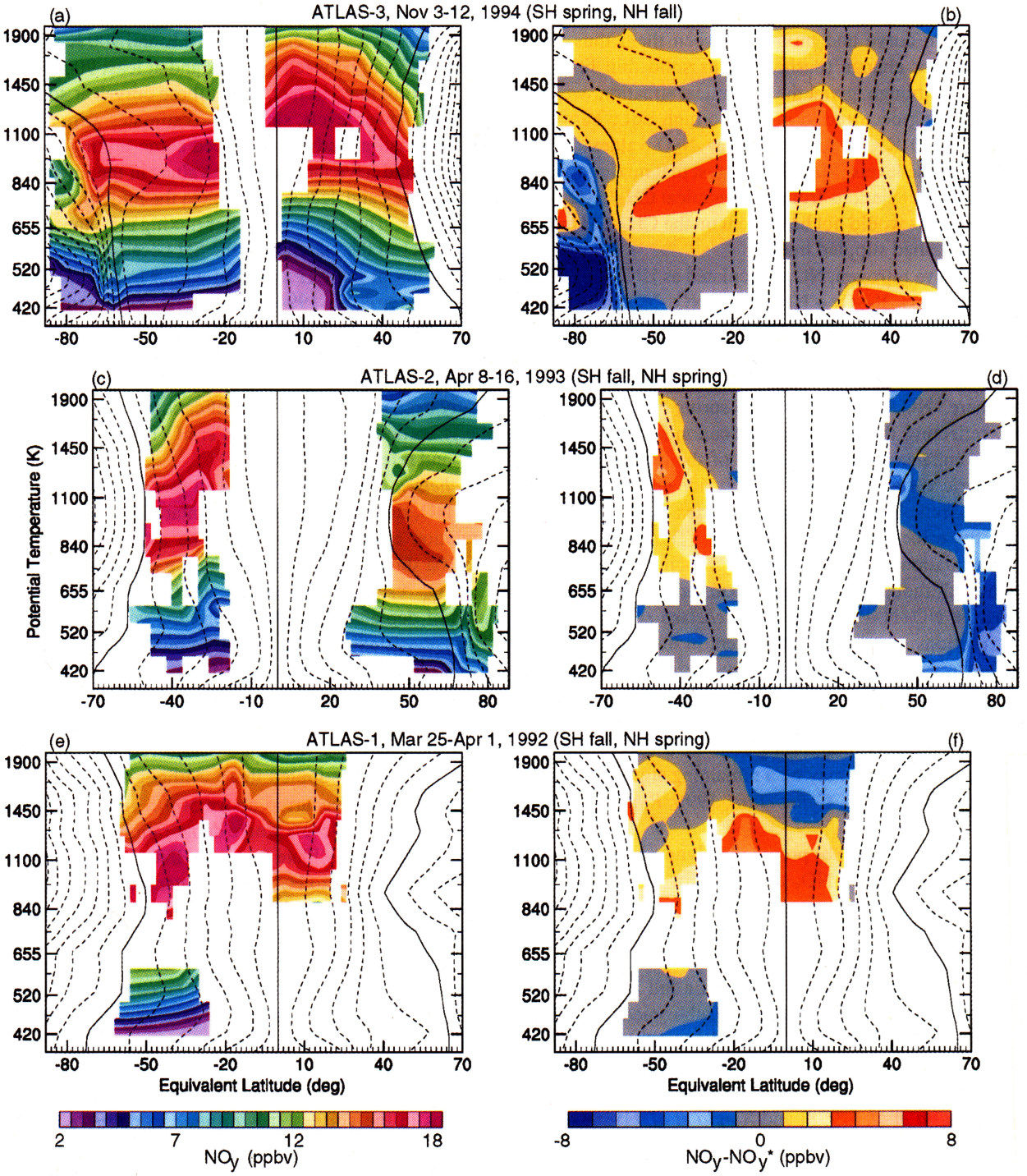


**Plate 10.** Same as Plate 3, but for EqL/θ space fields of ATMOS (left) $NO_y$ and (right) $NO_y$-$NO_y^*$.

tex below ~800 K had experienced mixing, with the greatest changes seen in the vortex interior between ~500 and 600 K. A given deficit in $CH_4$-$CH_4^*$ represents more mixing in the NH plot than in the SH plot; since the horizontal $N_2O$ gradients were weaker in the NH, air masses that were separated by the same physical distance are represented by points more closely spaced around the nonlinear portion of the correlation curve and mixing between them thus produces a smaller change (dashed versus solid thin lines in Figure 1a). Although, given the dynamical situation, we expect that mixing occurred in middle to high EqLs between ~800 and 1100 K, the uniformly low $N_2O$ values (~10-50 ppbv) at these levels (Plate 3c) suggest that mixing would not cause large deviations from the canonical $CH_4/N_2O$ correlation and thus would not be evident on the $CH_4$-$CH_4^*$ map (Figure 1a, dashed stippled line).

Total reactive nitrogen, $NO_y$, calculated as $HNO_3 + NO + NO_2 + ClONO_2 + 2N_2O_5 + HNO_4$, and $NO_y$-$NO_y^*$ (Plate 10) are also useful for examining aspects of transport and chemistry in the polar stratosphere [e.g., *Michelsen et al.*, 1998b; *Rinsland et al.*, 1999, and references therein]. In the lower stratosphere, $NO_y$ in the Antarctic spring vortex was depleted, reflecting the severe denitrification seen in Plate 5. $NO_y$ was enhanced along the edge of the Antarctic lower stratospheric vortex relative to that outside during AT-3 and inside the Arctic lower stratospheric vortex during AT-2, reflecting the effects of diabatic descent. The net source of $NO_y$ is oxidation of $N_2O$ by $O(^1D)$, which increases with increasing altitude; above about 30 km there is fast loss via the reaction $NO+N \rightarrow N_2+O$ [e.g., *Michelsen et al.*, 1998b]. These reactions, combined with ascent in the tropics, poleward and downward transport in the winter hemisphere, and mixing in midlatitudes, result in the overall pattern of $NO_y$ with a maximum in the tropical middle stratosphere. The minimum in the Antarctic during AT-3 near 840 K and the maximum just below it may be a remaining signature of descent in the vortex [e.g., *Callis et al.*, 1996; *Rinsland et al.*, 1996a, 1999].

*Michelsen et al.* [1998b] provided polynomial fits to correlation curves between $NO_y$ and $N_2O$ for the tropics, the midlatitudes in fall, the high-latitude extravortex region in spring, the protovortex, and the Arctic vortex. We use the protovortex relationship to calculate $NO_y^*$ and $NO_y$-$NO_y^*$, because it is the best estimate available of a fall high-latitude relationship uninfluenced by tropical/subtropical air. The protovortex correlation curves derived for AT-2 in the SH and AT-3 in the NH are nearly the same [*Michelsen et al.*, 1998b]. $NO_y$-$NO_y^*$ obtained using the relationships for $NO_y^*$ given by *Sugita et al.* [1998] and *Kondo et al.* [1999] (who used a relationship derived from AT-3 NH observations including protovortex, midlatitude, and low-latitude air) is qualitatively similar, with small quantitative differences in the middle EqL upper and lower stratosphere. Figure 1b shows schematically the $NO_y^*$ curve and examples of mixing lines. The fall correlation curve between $N_2O$ and $NO_y$ is nonlinear for low $N_2O$, with a maximum near $N_2O \approx$ 45 ppbv [e.g., *Michelsen et al.*, 1998b]. Where air masses from points on either side of the maximum are in close physical proximity (such as inside and outside the spring polar vortices), changes in the correlation curve, indicated in Plate 10 by departures of $NO_y$-$NO_y^*$ from zero, will result from mixing between those air masses [*Waugh et al.*, 1997] (Figure 1b). Examination of individual $N_2O$ profiles shows that vortex and extravortex air will fall on either side of the peak in $NO_y$ at levels between ~510 K and 900 K in the SH during AT-3 and between ~475 K and at least 900 K during AT-2. Mixing may, in fact, affect these curves at somewhat higher and lower levels, since these estimates were based on fields that had already experienced some mixing; previous mixing would have increased the values in the lower stratospheric vortex and decreased those in the midlatitude middle stratosphere. The effects of earlier mixing are expected to be much larger in the NH than in the SH because of the greater permeability of the NH vortex in winter [e.g., *Plumb et al.*, 1994; *Manney et al.*, 1994c, and references therein]. Departures of $NO_y$-$NO_y^*$ from zero may also result from denitrification via sedimentation of PSCs (Figure 1b, thin stippled dashed line), and changes in $N_2O/NO_y$ correlations have frequently been used to infer denitrification in the lower stratospheric vortices [e.g., *Michelsen et al.*, 1998b; *Kondo et al.*, 1999, and references therein].

*Michelsen et al.* [1998b] showed that approximately half of the $NO_y$ deficit apparent in the Antarctic vortex $NO_y/N_2O$ correlation curve for AT-3 could be attributed to mixing. Plate 10a shows the morphology of the regions of depressed $NO_y$-$NO_y^*$ resulting from mixing and/or denitrification. The region of depleted $NO_y$-$NO_y^*$ along the vortex edge during AT-3 is consistent with the effects of mixing, showing a similar pattern to that seen in $CH_4$-$CH_4^*$. Most of the depression in $NO_y$-$NO_y^*$ in the Antarctic vortex below 500 K can be attributed to denitrification, since mixing at the high $N_2O$ values there would not change the correlation curve (Figure 1b, thick solid stippled line). Although we have shown that some mixing occurred above 500 K, denitrification is also expected at all levels where dehydration occurred, up to at least about 600 K (Plate 8), since $HNO_3$ is expected to be removed in addition to $H_2O$ when water ice PSCs sediment. This is consistent with the vertical extent of the region of most strongly depressed $NO_y$-$NO_y^*$ in Plate 10.

In the Arctic vortex during AT-2, $N_2O$ values were low enough and gradients across the vortex edge strong enough that $NO_y$-$NO_y^*$ would be altered by mixing at levels down to at least 475 K; mixing would probably be apparent at somewhat lower levels, since considerable mixing prior to AT-2 [e.g., *Manney et al.*, 1994c] had already increased $N_2O$ mixing ratios in the vortex. It is difficult to define a top level where extravortex $N_2O$ was greater than 50 ppbv during or prior to AT-2 because of the large area of coverage of air either currently or recently inside the vortex in the middle stratosphere (section 2). Comparing the Arctic lower stratospheric vortex region with the region of mixing indicated in Plate 9, and given that it is not necessary to invoke denitrification to explain the vortex $NO_y/N_2O$ correlation during AT-2 since that correlation fell on a mixing line like the

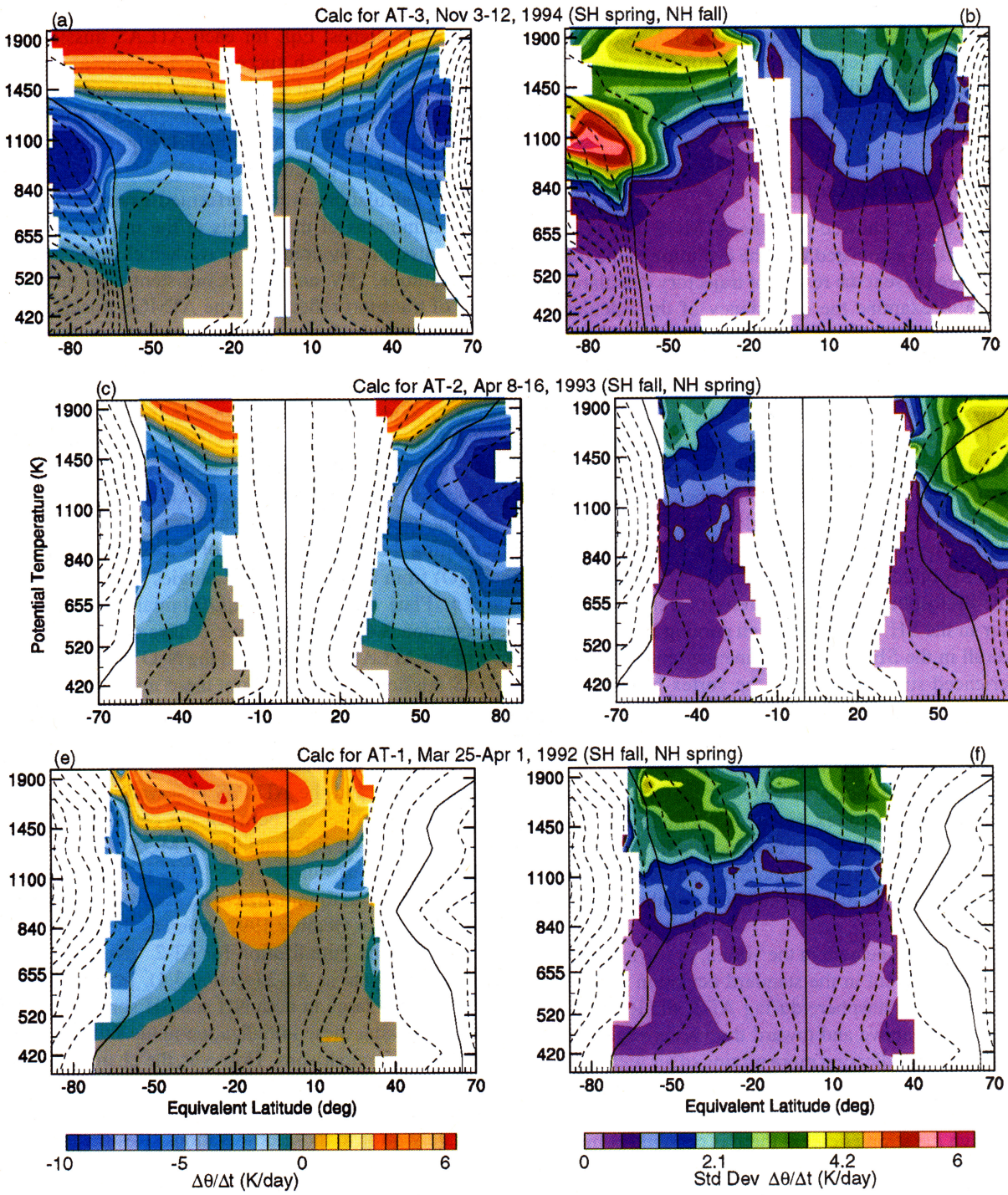


**Plate 11.** Same as Plate 3, but for EqL/θ space fields of (left) the change in potential temperature and (right) the standard deviation of that change calculated for parcels initialized in columns at the latitude and longitude of each ATMOS observation (see section 3.3), from 32-day back trajectory calculations. The change in potential temperature is expressed in K/d by dividing the change for each parcel by 32 before gridding in EqL/θ space.

dashed black line in Figure 1b [*Michelsen et al.*, 1998b], the decrease in $NO_y$-$NO_y^*$ below ~800 K leads us to believe that mixing with extravortex air took place throughout the portion of the vortex observed by ATMOS. A signature of mixing can also be seen from 800–1100 K; this was not evident in Plate 9 because the canonical $NO_y/NO_y^*$ correlation is much more sharply peaked than that for $CH_4$ and $N_2O$ (compare thick dashed stippled lines in Figures 1a and 1b), thus producing a greater change in $NO_y$ for these low $N_2O$ values.

### 4.3. Parcel History Calculations

The above results showed how the ATMOS data reflect transport processes associated with the evolution of the polar vortex. Here we present the results of trajectory calculations (section 3.3) to examine the consistency of the calculated history with the morphology of the ATMOS tracer fields.

Plate 11 summarizes the vertical motion experienced by the air measured by ATMOS in the 32 days prior to each ATLAS mission. Consistent with the calculations of *Manney et al.* [1994c], strong descent was still occurring in the spring middle stratosphere, although there was net ascent in the upper stratosphere. The values shown here represent the calculated descent of the air sampled by ATMOS averaged in PV/θ bins. The region of stronger but more localized descent in the SH middle stratosphere during AT-3 than in the NH middle stratosphere during AT-2 reflects greater confinement of air in the SH vortex; although cooling rates are not larger overall in the SH, greater confinement means that air that experienced strong descent in the vortex has not been mixed with less-descended midlatitude or subtropical air. The abrupt increase in descent in crossing into the vortex at levels below 840 K (where the vortex is still well defined) in both hemispheres also indicates a greater uniformity of the averaged air within the vortex, since the cooling rates themselves do not increase so dramatically across this boundary. That this increase is stronger in the SH than in the NH reflects the greater degree of impermeability of the Antarctic vortex.

The effects of confinement in the vortex, or in vortex remnants, are also apparent in the standard deviation of $\Delta\theta/\Delta t$. In the SH middle stratosphere during AT-3, the location of largest variance is above and toward the vortex edge of the maximum descent, indicating more mixing of air with differing descent rates along the vortex edge and where the vortex is more eroded. A similar pattern occurs in the NH during AT-2, although the strong descent there is centered at higher levels. An increase in the standard deviation along the vortex edge in the SH extends only down to about 650 K, below which the vortex is still quite strong, suggesting greater mixing along the vortex edge at levels where it has been eroded. Both Arctic and Antarctic vortices show more descent along the vortex edge in the lower stratosphere, consistent with previous studies [e.g., *Schoeberl et al.*, 1992; *Manney et al.*, 1994c; *Eluszkiewicz et al.*, 1995] and with the appearance of the ATMOS tracer fields (e.g., Plates 3 and 5). The descent rates at the lowest levels shown are near zero in the NH vortex, but in the SH there is ascent of $\lesssim$0.4 K/d in the interior of the Antarctic vortex (in the grey contour region in Plate 11).

In the fall hemisphere a widespread region of descent is centered at highest EqL for each ATLAS mission, with stronger descent in each succeeding mission, as expected from the more advanced season of the later missions. The variance decreases in the upper stratosphere at the highest EqLs for AT-3 but not for AT-2 or AT-1, suggesting confinement in the protovortex during AT-3.

Similar calculations were performed examining the net horizontal motions of the parcels in the month before the ATLAS missions, by computing average changes and variance in latitude, sPV, and EqL. Consistent with the overall picture of transport reflected in the ATMOS tracers, the results of these calculations (not shown) indicate large variance along the vortex edge between ~600 and 900 K in the SH during AT-3 and at all levels below ~900 K in the NH during AT-2, an increase in variance in the NH during AT-2 at all EqLs between ~850 and 1100 K, and a distinct decrease in variance at the highest northern EqLs for the fall AT-3 observations that is not apparent during AT-2 or AT-1.

Similar averages were calculated from the 32-day histories plotting the historical values of trace gases ($N_2O$, $CH_4$, and $H_2O$) from the EqL/θ "climatologies" described in section 3.4. Plate 12 shows the EqL/θ initialization fields for $N_2O$ (section 3.4), averaged over 8 days centered 32 days prior to the ATLAS missions, and the $N_2O$ at the time of the ATLAS missions calculated from these initialization fields. Given the idealized nature of the initialization fields and biases between the ATMOS and UARS data [e.g., *Roche et al.*, 1996], we do not expect quantitative agreement between the calculated fields and the ATMOS observations. The overall systematic differences between the calculated fields in Plate 12 (right-hand side) and the ATMOS $N_2O$ in Plate 3 are, in fact, greatest during AT-3. This is not unexpected, since the fields used to initialize that case were derived from CLAES data from October 1992, whereas the CLAES data used to derive the initialization for AT-2 were from March 1993, the same year as AT-2 (section 3.4). Interannual variability, which is large in both NH and SH spring, thus contributes to making these initialization fields suitable mainly for qualitative comparisons. However, the changes between the initial and final fields help to illuminate the mechanisms that shaped the air masses sampled by ATMOS in the month immediately prior to those observations. Results for initialization with fields derived from CLAES $CH_4$ and MLS $H_2O$ (not shown) are similar to those for $N_2O$.

Continuing descent along the vortex edge (Plate 11) leads to a decrease in $N_2O$ values in the lower stratosphere; weak ascent in the vortex interior leads to a slight increase in the interior of the vortex (compare Plates 12a and 12b (SH) and Plates 12c and 12d (NH)). The pattern thus produced is consistent with the pattern seen more strongly in the ATMOS data (Plate 3). The history for the entire winter probably

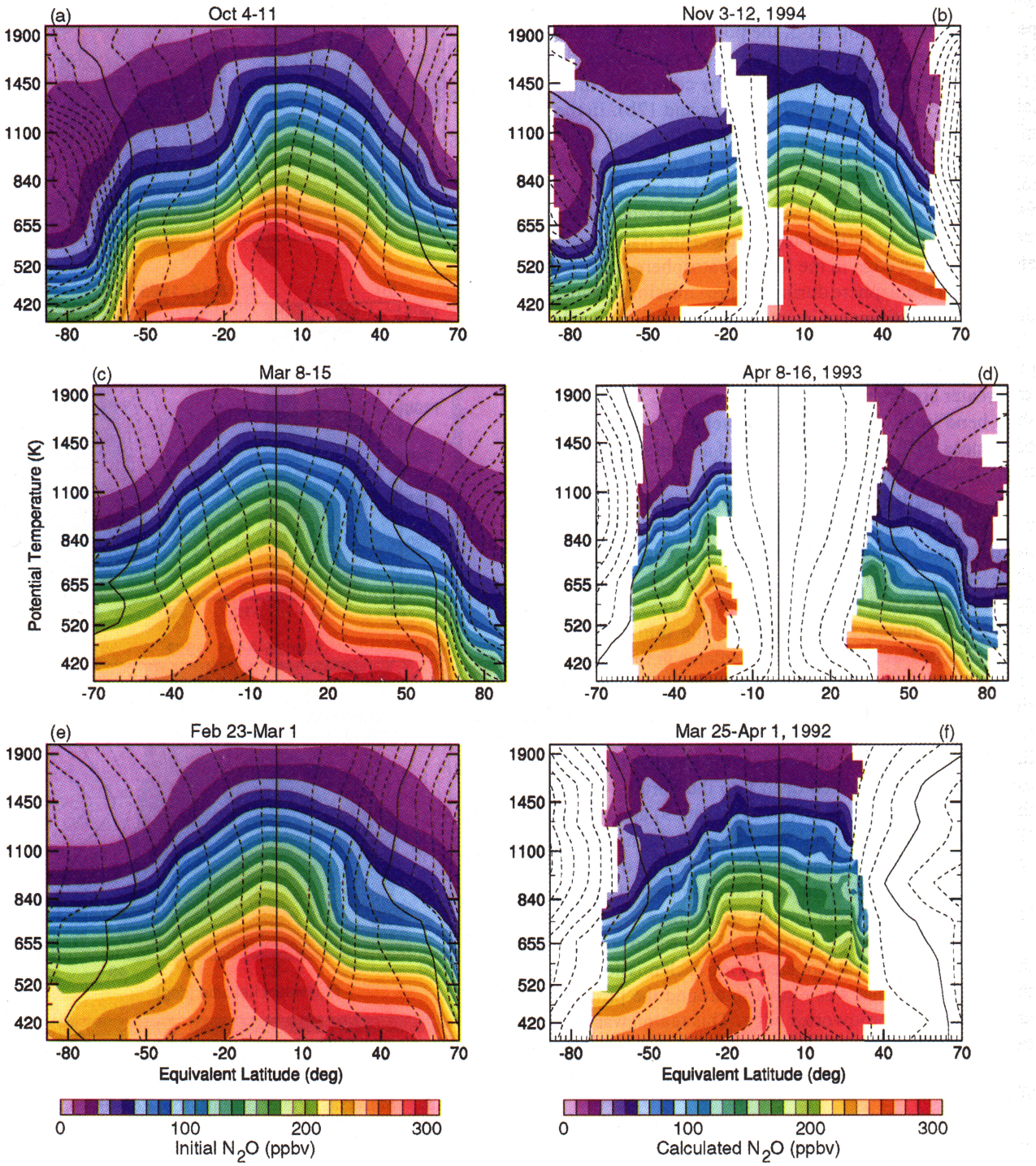


**Plate 12.** Same as Plate 3, but for EqL/θ space fields of (left) initialization $N_2O$ data derived from Cryogenic Limb Array Etalon Spectrometer (CLAES) observations (section 3.4) and (right) $N_2O$ calculated from these initialization fields for the time of the ATMOS observations. The transport calculations use parcels initialized in columns at the latitude and longitude of each ATMOS observation, as described in section 3.3, and are 32 days long.

also contributes to the pattern seen in the ATMOS data, since strongest descent in the lower stratosphere is along the vortex edge throughout the winter in the SH and during the late winter in the NH [e.g., *Manney et al.*, 1994c]. In the SH upper stratosphere during AT-3, the poleward spread of higher $N_2O$ values results from mixing as the polar vortex decays (the extent of the decay can be seen by comparing the overlaid |sPV| contours between Plates 12a and 12b). In the NH middle stratosphere during AT-2, spreading and poleward excursion of the $N_2O$ contours indicate the strong mixing taking place there in the month preceding the AT-2 observations. The evolution of the vortices and associated tracer transport results in further steepening of the tracer gradients along the vortex edge in the lower stratosphere.

In the fall hemisphere during all three missions, increasing descent and confinement in the polar regions lead to downward motion of the tracer contours. This motion is most pronounced during AT-3, consistent with stronger descent and greater confinement during that mission. During AT-2 a sharp bend in the $N_2O$ contours develops between 520 and 655 K near 40°S EqL, reminiscent of a similar bend seen in the AT-2 data (Plate 3).

The standard deviation of the $N_2O$ values comprising the average in each PV/θ grid box (Plate 13) shows enhanced mixing along the Antarctic vortex edge during AT-3 above ~600 K, along the Arctic vortex edge during AT-2 below ~840 K, and in most of the NH region between 840 and 1100 K during AT-2. Because the initial $N_2O$ field (Plate 12c) had weak horizontal gradients in the Arctic vortex during AT-2, the decrease in variance in the vortex interior does not necessarily indicate the absence of mixing, but it does suggest that mixing during this period may have been limited to air from near the vortex edge, rather than having extravortex air transported deep into the vortex. Although the variations in ATMOS $CH_4$-$CH_4^*$ (Plate 9) and $NO_y$-$NO_y^*$ (Plate 10) reflect processes that occurred throughout the winter, there is fair agreement between the areas of enhanced mixing seen in ATMOS tracer relationships and the calculated diagnostics of recent mixing shown here.

In the fall hemisphere a region of increased variance in the high EqL upper stratosphere during each mission reflects the mixing of air that was drawn in around the protovortex and drawn off the protovortex edge. This region was smaller during AT-3 than during the previous missions, indicating a stronger transport barrier and more limited mixing during AT-3.

We now look in more detail at the recent history of the air observed by ATMOS in the spring vortices and the fall protovortices. We show the positions (in PV and Δθ) and $N_2O$ values (from the idealized UARS-based fields) of individual parcels that were in specified PV/θ bins at the time of the ATMOS observations. We also show the averages for groups of parcels initialized at the same level; the close correspondence between these averages (of 121 parcels each) and the individual parcels indicates that these displays are representative of the behavior of the ensemble of parcels.

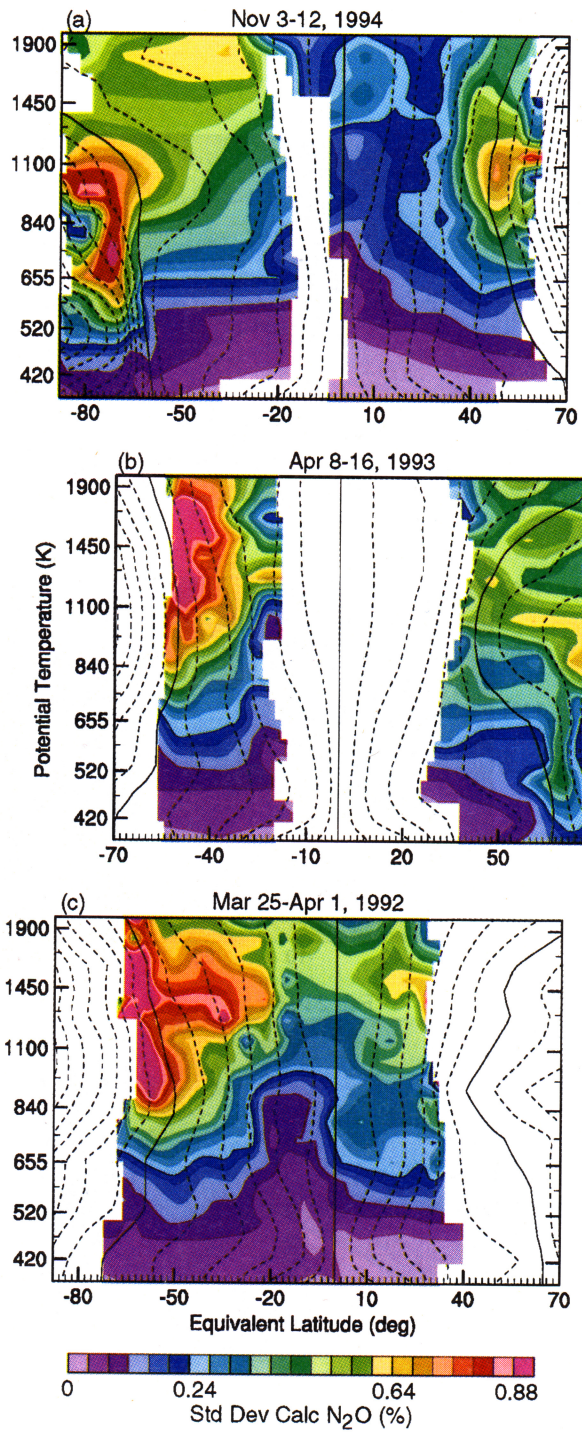


**Plate 13.** Same as Plate 3, but for EqL/θ space fields of the standard deviation of the calculated $N_2O$ shown in Plate 12. The standard deviation is normalized by the average (Plate 12, right) to emphasize relative changes.

Plate 14 shows such a plot at several levels for the AT-3 sunrise observation locations between -1.6 and -2.0 $\times 10^{-4}$ $s^{-1}$ sPV; this range is inside the vortex but still in the region of strong PV gradients, as can be seen in the sPV overlays on the EqL/θ plots. Below 445 K (Plate 14a), there

was overall ascent, as mentioned above, with increasing descent with increasing altitude above that (Plates 14b, 14c, and 14d). At levels below 485 K, the sPV that the parcels came from is limited to a small range closely centered on the values at the time of AT-3 (denoted by vertical bars), as in Plate 14a, indicating very limited mixing in this sPV range. Between ~500 and 800 K (including the ranges shown in Plates 14b and 14c) there is increasingly more mixing, with air having come from both well outside and well inside the vortex (both much lower and much higher |sPV|). Although the situation is somewhat similar at 800-875 K (Plate 14d), the majority of the air came from higher |sPV| values; at these levels the major changes during the period were due to the strong erosion of the vortex, as can be seen in Plate 12.

Plate 15 shows similar plots in the lower stratosphere for locations deep inside the vortex ($|sPV| > 2.0 \times 10^{-4}$ s$^{-1}$) and along the vortex edge ($1.0 < |sPV| < 1.6 \times 10^{-4}$ s$^{-1}$). In the vortex interior (Plate 15a), ascent extends up to ~500 K and limited mixing is indicated by the tight clustering of the parcels near the |sPV| region where AT-3 observed them. The slight extension of these parcels' positions toward lower |sPV| suggests some mixing with air from outside the vortex core, but there is no evidence of air from outside the vortex ($|sPV| < 1.0 \times 10^{-4}$ s$^{-1}$). Higher up in the vortex interior (Plate 15b), most parcels came from much higher |sPV|, reflecting substantial vortex erosion in the month preceding AT-3. There is continuing weak descent in the lower stratosphere, and a considerable amount of extravortex air mixes into the vortex edge region down to at least 380 K (e.g., Plate 15c), consistent with the calculations of *Pierce et al.* [1994]. Below ~420 K the $1.0 < |sPV| < 1.6 \times 10^{-4}$ s$^{-1}$ range extends farther into the vortex interior, since the strongest PV gradients at those levels are at slightly lower |sPV| values; the presence of extravortex air in this |sPV| range at the lowest levels studied thus indicates mixing well into the vortex interior. In the midstratosphere (Plate 15d) the air in the vortex edge region came from a wide range of sPV, both deep inside and well outside the vortex, with most of the air coming from lower |sPV| (outside the vortex); the air coming from the vortex interior experienced strong descent.

Plate 16 shows the origins of parcels that were at the locations of AT-2 observations in the interior of the Arctic vortex ($sPV > 1.6 \times 10^{-4}$ s$^{-1}$) in the lower and middle stratosphere. In contrast to the SH, there was still weak descent in the vortex interior during AT-2 below 500 K. There are indications of more mixing at these levels in the NH than in the SH during AT-3, with much of the air at the lowest levels shown here coming from deeper in the vortex, but some also coming from well outside the vortex (Plate 16a). In the midstratosphere (Plate 16b) there is strong mixing in this region, with large portions of the air coming from both deep in the vortex and from the vortex exterior.

Plate 17 shows similar plots for air along the vortex edge and in the outer part of the vortex ($1.2 < sPV < 1.6 \times 10^{-4}$ s$^{-1}$). The spread in the parcel positions indicates strong mixing at all levels where the vortex can still be defined. There was considerably more mixing of both extravortex and inner vortex air at the lowest levels (below 500 K) in the NH during AT-2 than in the SH during AT-3.

Finally, we compare the parcel histories in the fall protovortex edge region ($1.0 < |sPV| < 1.2 \times 10^{-4}$ s$^{-1}$) for the three ATLAS missions (Plate 18). At all the levels shown, most of the parcels (during all three missions) came from lower |sPV|, since PV values within the developing vortex are increasing. Since AT-2 had less coverage of the protovortex than did AT-1 and AT-3 (e.g., section 2), some differences between AT-2 and the other missions are expected; however, these differences, while resulting from sampling rather than physical effects, should be reflected in the ATMOS observations. In the middle to lower stratosphere (e.g., Plates 18a, 18b, and 18c) the histories were similar for all three missions, with nearly equal average descent, strongest descent in parcels from higher |sPV|, and similar ranges of $N_2O$. Between 870 and 950 K (Plates 18d, 18e, and 18f) a difference in the descent rates between the three missions is apparent, with slightly greater average descent during AT-3 than during AT-2 and greater descent during AT-2 than during AT-1. The difference in descent between AT-3 and AT-1 was even more pronounced in the upper stratosphere (e.g., Plates 18g, 18h, and 18i), although there is still only a slight difference between AT-3 and AT-2. Above ~870 K during AT-1 (Plates 18f and 18i), there were parcels in the protovortex edge region that had come from the tropics (near zero sPV) and that had experienced net ascent along their paths in the month preceding AT-1. Although AT-3 also observed parcels that originated in the tropics (Plates 18d and 18g), they had all experienced net descent over the previous month. AT-2 did not sample any tropical air in the protovortex region. This is related to the more symmetric and quiescent protovortex during AT-2 than during AT-3 and AT-1 (section 2), which not only contributed to poorer sampling of the protovortex but also meant that less air was drawn into high latitudes from the tropics. Lowest average upper stratospheric $N_2O$ values during AT-2 (Plate 18h) and highest during AT-1 (Plate 18i) are consistent with the relative $N_2O$ values observed by ATMOS in the high-EqL upper stratosphere (Plate 3).

## 5. Summary and Conclusions

Trace gas fields measured by ATMOS during the three ATLAS missions have been mapped into equivalent latitude/θ space to examine how the tracer morphology is related to the evolution of the polar vortex. The highly distorted spring vortices result in coverage of subtropical to polar equivalent latitudes (EqLs). Although the fall protovortices are less asymmetric, there is enough variability to extend the coverage ~10° poleward in EqL from the highest geographical latitude observed. These fields and similar mappings of derived fields (e.g., $NO_y$, $H_2O+2CH_4$, etc.) allow us to examine the effects of transport, mixing, and chemical processes in and around the polar vortex in more detail than previous studies and to compare conditions for fall and spring between missions. The ATMOS EqL/θ fields

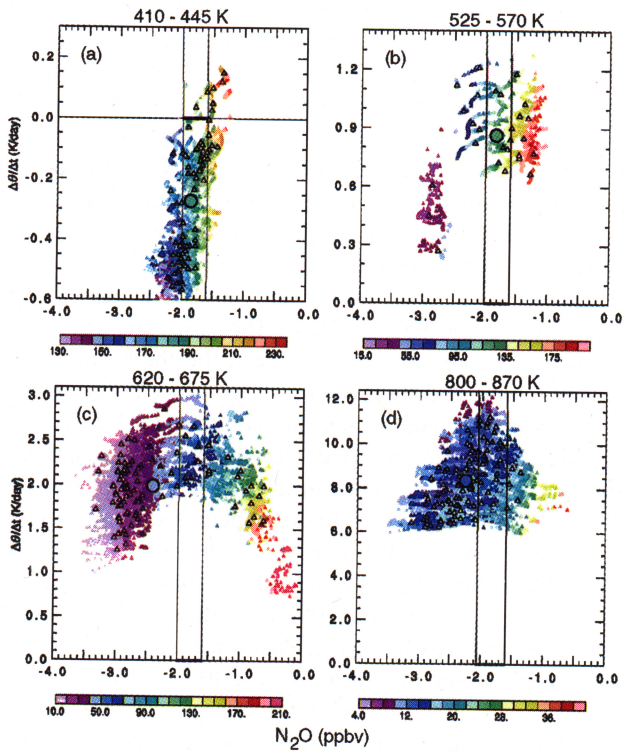


**Plate 14.** History of parcels for AT-3 sunrise (SH) observations with |sPV| between 1.6 and 2.0 × $10^{-4}$ $s^{-1}$ at (a) 410-445 K, (b) 525-570 K, (c) 620-675 K, and (d) 800-870 K. The *x* axis is sPV ($10^{-4}$ $s^{-1}$); the *y* axis is the change in theta expressed in K/d by dividing the change for each parcel by 32 days, with positive values indicating descent (i.e., parcels that came from above their location at the time of the ATMOS observations appear above zero on the plot). Parcels are color coded by their $N_2O$ mixing ratio (ppbv), calculated from the idealized UARS-based fields described in section 3.4. Small colored triangles show individual parcels' positions 32 days prior to the ATMOS observations. Small colored triangles with black borders represent the average for the 121 parcels initialized at a single level for each ATMOS profile (see section 3.3). Large colored circles with black borders circles represent the average position of all the parcels included. Vertical bars show the |sPV| range of the ATMOS profile locations that were included in each plot; the horizontal line shows zero theta change. Each theta range is chosen to include 5 of the 100 levels at which parcels were initialized, a vertical distance comparable to the ATMOS vertical resolution. Note that different $N_2O$ color scales are used for each level to emphasize the range of variations in $N_2O$ .

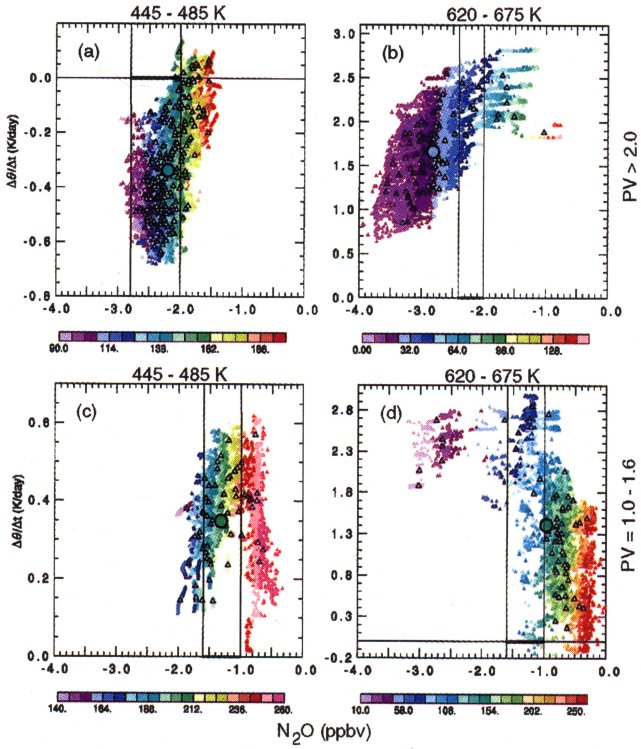


**Plate 15.** Same as Plate 14, but for (a and b) |sPV| greater than 2.0 × $10^{-4}$ $s^{-1}$ (vortex core) and (c and d) |sPV| between 1.0 and 1.6 × $10^{-4}$ $s^{-1}$ (vortex edge region).

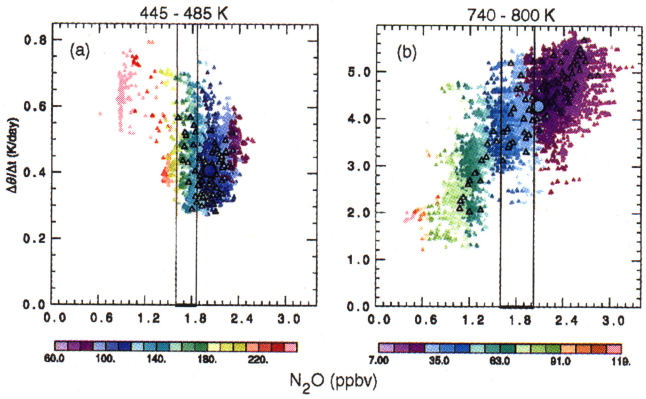


**Plate 16.** Same as Plate 14, but for AT-2 sunrise (NH) observations with sPV greater than 1.6 × $10^{-4}$ $s^{-1}$.

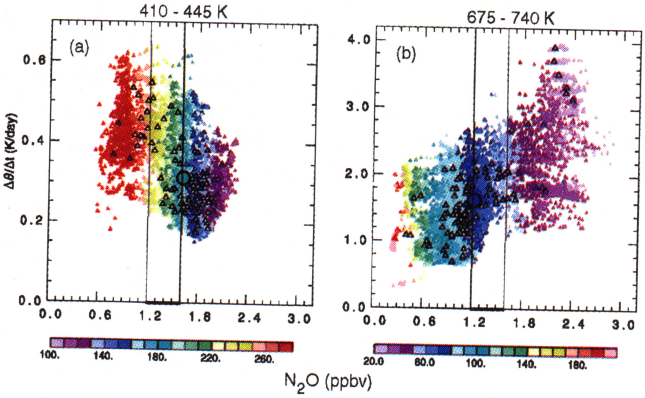


**Plate 17.** Same as Plate 14, but for AT-2 sunrise (NH) observations with sPV between 1.2 and 1.6 × $10^{-4}$ $s^{-1}$.

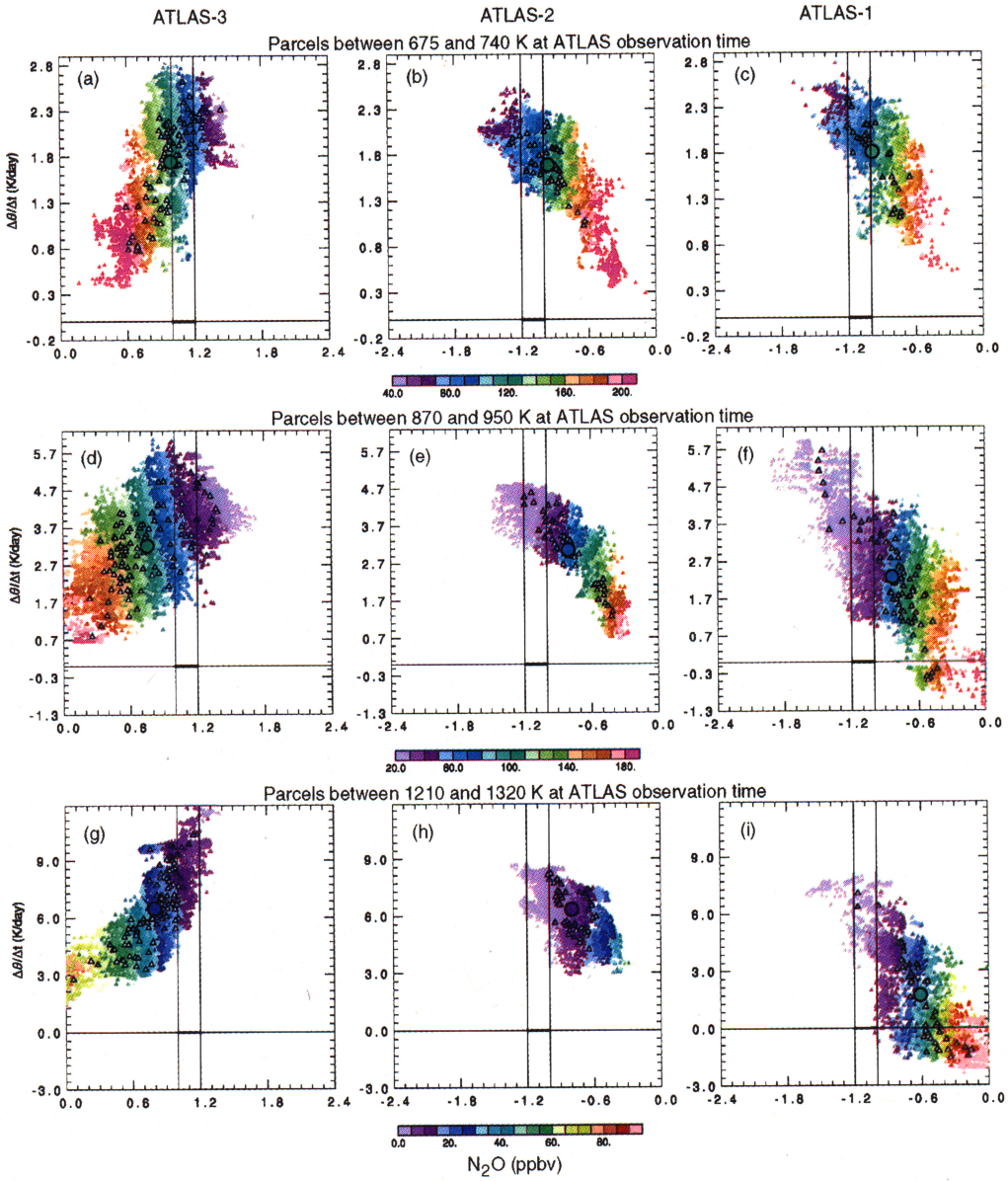


**Plate 18.** Same as Plate 14, but for |sPV| between 1.0 and 1.2 × $10^{-4}$ $s^{-1}$ for fall (sunset) observations during each of the ATLAS missions.

are compared with the results of back trajectory calculations simulating the history of the air measured by ATMOS.

The EqL/θ fields of long-lived tracers in the spring hemisphere during AT-3 and AT-2 show the effects of descent that has taken place throughout the winter in the confined region of the polar vortex, as noted in previous studies [*Abrams et al.*, 1996a, c, and references therein]. The net effect of strong descent in the upper stratosphere and decreasing descent with decreasing altitude is apparent in the packing of the tracer contours in the lower stratosphere. In addition, the EqL/θ mapped fields reveal evidence of greater descent at the edge of the lower stratospheric vortex than in the vortex center in both hemispheres, with tracer contours showing a downward excursion along the vortex edge. The results of trajectory calculations for the month prior to AT-3 and AT-2 are consistent with these patterns, showing continuing descent in the middle and upper stratosphere and along the vortex edge in the lower stratosphere, with weak ascent in the SH lower stratospheric vortex interior during AT-3.

In the SH middle and upper stratosphere during AT-3, the region of low (descended) tracer values is confined to a smaller region near the pole as altitude increases, indicating the effects of mixing and decay of the vortex. In the NH middle stratosphere during AT-2 the vortex was in the process of breaking down in a dramatic and untidy fashion, with a substantial portion of the vortex material pulled out into midlatitudes and mixed around and in the anticyclone. This process resulted in a spreading of low tracer values over a broad EqL range and weakening of vertical tracer gradients in the middle stratosphere.

Evidence of mixing in the spring lower stratospheric vortices is shown in variations of $CH_4$-$CH_4^*$ and $NO_y$-$NO_y^*$, where $CH_4^*$ and $NO_y^*$ are calculated from fall protovortex correlations with $N_2O$ [*Michelsen et al.*, 1998a]. The results show strong mixing in the SH during AT-3 above about 500 K, with the strongest mixing being confined to the vortex edge region between 500 and 700 K, consistent with calculations of mixing in the vortex edge region [e.g., *Pierce et al.*, 1994]. Strong mixing is indicated throughout the AT-2 Arctic vortex below about 850 K and at all EqLs covered between ~850 and 1100 K. Parcel history calculations for the month prior to the ATLAS missions show similar patterns of mixing. Trajectory calculations also indicate widespread mixing in the SH middle stratosphere above ~900 K during AT-3. Parcel histories for AT-3 show that air inside the vortex above ~500 K originated both deeper inside the vortex and well outside the vortex. Below that level the calculations indicated little mixing of vortex interior with extravortex air during AT-3, although air near the vortex edge (inside) did mix with extravortex air down to 380 K. In the Arctic during AT-2, trajectory calculations confirmed enhanced mixing along the vortex edge up to ~840 K and at all EqLs sampled by ATMOS above that; parcel histories showed extravortex air mixing well into the vortex above ~450 K and into the vortex edge region down to 380 K.

Strong denitrification in the SH vortex during AT-3 is evident in the EqL/θ $HNO_3$ field, which suggested that denitrification extended up to at least ~600 K. The morphology of $HNO_3$ in the Arctic lower stratospheric vortex during AT-2 is consistent with the effects of descent. If denitrification greater than ~1 ppbv had occurred, its effects should be visible in this plot; thus the EqL/θ-mapped $HNO_3$ field during AT-2 suggests that there was not significant denitrification during the 1992-1993 Arctic winter, consistent with previous studies [e.g., *Michelsen et al.*, 1998b; *Santee et al.*, 1999, and references therein]. Since the $NO_y/N_2O$ correlation is strongly affected by mixing over an even larger region than the $CH_4/N_2O$ correlation, little additional information regarding denitrification is obtained by examining $NO_y$-$NO_y^*$. Large decreases in $NO_y$-$NO_y^*$ in the interior of the Antarctic vortex below about ~600 K during AT-3 are likely due mainly to denitrification, although the decreases along the vortex edge at these levels may also result from mixing; below ~500 K the decrease can be attributed to denitrification, since other diagnostics indicate no substantial mixing into the vortex interior at those levels. During AT-2, in contrast, since there was evidence of mixing throughout the Arctic lower stratospheric vortex, the decrease in $NO_y$-$NO_y^*$ offers no unequivocal evidence of denitrification.

EqL/θ mapped $H_2O$ fields show strong dehydration in the Antarctic vortex during AT-3. Examination of $H_2O+2CH_4$ (which is unchanged by mixing and descent throughout the extratropical middle and lower stratosphere) indicates that Antarctic dehydration extended up to ~600 K during AT-3 and suggests the possibility of a small amount of dehydration in the Arctic vortex during AT-2 below ~500 K.

EqL/θ $O_3$ fields show strong $O_3$ depletion in the Antarctic spring vortex during AT-3 and evidence of $O_3$ loss in the Arctic vortex during AT-2. In the SH middle stratosphere during AT-3, EqL/θ $O_3$ fields in middle EqLs depart from expectations because many of the ATMOS observations at low PV were taken in a low ozone pocket, which forms when low-latitude, high-$O_3$ air is drawn into and confined in the anticyclone for a number of days, allowing $O_3$ mixing ratios to relax to much lower values. Photochemical mechanisms that depend primarily on solar conditions unrelated to vortex shape must thus be considered when analyzing maps of chemically active species in EqL/θ coordinates.

During fall the largest differences in the tracer fields between the three ATLAS missions stem from the fact that the vortex was further developed in each succeeding mission. Both EqL tracer fields and calculations indicated progressively greater average descent of the air in the protovortex region for AT-1, AT-2, and AT-3. The differences in average descent result from both larger radiative cooling rates and greater isolation of air in the protovortex (which led to less mixing of air that had experienced strong descent with air that experienced weaker descent) in the later missions. During both AT-3 and AT-1, air that originated in the tropics in the month preceding the mission was sampled in the protovortex edge region, consistent with large tongues of low-latitude air being drawn up around the protovortex; whereas during AT-1 some of this air experienced net ascent in the previous month, during AT-3 all of the air originally from the tropics experienced net descent, confirming greater downward motion prior to AT-3. During AT-2 the protovortex was more quiescent and ATMOS did not sample tropical air in the protovortex edge region.

The EqL/θ mapping of ATMOS observations from the three ATLAS missions has provided a detailed view of transport in and around the spring polar vortices and the developing vortices in fall, and it has given a context for detailed comparison of fall and spring conditions between missions. These fields are also useful for other studies. They provide a common coordinate system for comparison of ATMOS observations with those from instruments that have simultaneous observations but different sampling patterns. Although the ATMOS observations do not provide complete global EqL coverage, the coverage is sufficient that these fields can be used for some model initializations. Ongoing studies using the EqL/θ-mapped ATMOS data for these purposes will provide additional insight into the processes shaping trace gas fields in the spring and fall stratosphere.

**Acknowledgments.** We thank the ATMOS, CLAES, and MLS instrument teams for their role in producing those data sets, especially H. C. Pumphrey for MLS $H_2O$ retrievals, and the UKMO (R. Swinbank and A. O'Neill) for meteorological data. Work at the Jet Propulsion Laboratory, California Institute of Technology, and the Lockheed Martin Advanced Technology Center was done under contract with the National Aeronautics and Space Administration. H.A.M. was supported by the NASA Atmospheric Chemistry, Modeling, and Analysis Program (NAS1-98118).

## References

Abbas, M. M., et al., The hydrogen budget of the stratosphere inferred from ATMOS measurements of $H_2O$ and $CH_4$, *Geophys. Res. Lett.*, *23*, 2405–2408, 1996a.

Abbas, M. M., et al., Seasonal variations of water vapor in the lower stratosphere inferred from ATMOS/ATLAS-3 measurements of $H_2O$ and $CH_4$, *Geophys. Res. Lett.*, *23*, 2401–2404, 1996b.

Abrams, M. C., et al., ATMOS/ATLAS–3 observations of long-lived tracers and descent in the Antarctic vortex in November 1994, *Geophys. Res. Lett.*, *23*, 2341–2344, 1996a.

Abrams, M. C., et al., On the assessment and uncertainty of atmospheric trace gas burden measurements with high resolution infrared solar occultation spectra from space by the ATMOS experiment, *Geophys. Res. Lett.*, *23*, 2337–2340, 1996b.

Abrams, M. C., et al., Trace gas transport in the Arctic vortex inferred from ATMOS ATLAS–2 observations during April 1993, *Geophys. Res. Lett.*, *23*, 2345–2348, 1996c.

Allen, D. R., J. L. Stanford, M. A. López-Valverde, N. Nakamura, D. J. Lary, A. R. Douglass, M. C. Cerniglia, J. J. Remedios, and F. W. Taylor, Observations of middle atmosphere CO from the UARS ISAMS during the early northern winter 1991/1992, *J. Atmos. Sci.*, *56*, 563–583, 1999.

Austin, J., R. R. Garcia, J. M. Russell III, S. Solomon, and A. F. Tuck, On the atmospheric photochemistry of nitric acid, *J. Geophys. Res.*, *91*, 5477–5485, 1986.

Bowman, K. P., Large-scale isentropic mixing properties of the Antarctic polar vortex from analyzed winds, *J. Geophys. Res.*, *98*, 23,013–23,027, 1993.

Brasseur, G., and S. Solomon, *Aeronomy of the Middle Atmosphere*, 2nd Ed., D. Reidel, Norwell, Mass., 1986.

Butchart, N., and E. E. Remsberg, The area of the stratospheric polar vortex as a diagnostic for tracer transport on an isentropic surface, *J. Atmos. Sci.*, *43*, 1319–1339, 1986.

Callis, L. B., D. N. Baker, M. Natarajan, J. B. Blake, R. A. Mewaldt, R. S. Selesnick, and J. R. Cummings, A 2-D model simulation of downward transport of $NO_y$ into the stratosphere: Effects on the 1994 austral spring $O_3$ and $NO_y$, *Geophys. Res. Lett.*, *23*, 1905–1908, 1996.

Dahlberg, S. P., and K. P. Bowman, Isentropic mixing in the Arctic stratosphere during the 1992–1993 and 1993–1994 winters, *Geophys. Res. Lett.*, *22*, 1237–1240, 1995.

Dunkerton, T. J., and D. P. Delisi, Evolution of potential vorticity in the winter stratosphere of January-February 1979, *J. Geophys. Res.*, *91*, 1199–1208, 1986.

Eluszkiewicz, J., R. A. Plumb, and N. Nakamura, Dynamics of wintertime stratospheric transport in the geophysical fluid dynamics laboratory SKYHI general circulation model, *J. Geophys. Res.*, *100*, 20,883–20,900, 1995.

Evans, S. J., R. Toumi, J. E. Harries, M. P. Chipperfield, and J. M. Russell III, Trends in stratospheric humidity and the sensitivity of ozone to these trends, *J. Geophys. Res.*, *103*, 8715–8725, 1998.

Fahey, D. H., S. Solomon, S. R. Kawa, M. Loewenstein, J. R. Podolske, S. E. Strahan, and K. R. Chan, A diagnostic for denitrification in the winter polar stratospheres, *Nature*, *345*, 698–702, 1990a.

Fahey, D. H., K. K. Kelly, S. R. Kawa, A. F. Tuck, M. Loewenstein, K. R. Chan, and L. E. Heidt, Observations of denitrification and dehydration in the winter polar stratospheres, *Nature*, *344*, 321–324, 1990b.

Fisher, M., A. O'Neill, and R. Sutton, Rapid descent of mesospheric air into the stratospheric polar vortex, *Geophys. Res. Lett.*, *20*, 1267–1270, 1993.

Froidevaux, L., et al., Validation of the UARS Microwave Limb Sounder ozone measurements, *J. Geophys. Res.*, *101*, 10,017–10,060, 1996.

Gunson, M. R., et al., The Atmospheric Trace Molecule Spectroscopy (ATMOS) experiment: Deployment on the ATLAS Space Shuttle missions, *Geophys. Res. Lett.*, *23*, 2333–2336, 1996.

Hintsa, E. J., et al., Dehydration and denitrification in the arctic polar vortex during the 1995-1996 winter, *Geophys. Res. Lett.*, *25*, 501–504, 1998.

Jones, R. L., J. A. Pyle, J. E. Harries, A. M. Zavody, J. M. Russell, and J. C. Gille, The water vapour budget of the stratosphere studied using LIMS and SAMS satellite data, *Q. J. R. Meteorol. Soc.*, *112*, 1127–1143, 1986.

Juckes, M. N., and A. O'Neill, Early winter in the northern hemisphere, *Q. J. R. Meteorol. Soc.*, *114*, 1111–1125, 1988.

Koike, M., N. B. Jones, W. A. Matthews, P. V. Johnston, R. L. McKenzie, D. Kinnison, and J. Rodriguez, Impact of Pinatubo aerosols on the partitioning between $NO_2$ and $HNO_3$, *Geophys. Res. Lett.*, *21*, 597–600, 1994.

Kondo, Y., et al., $NO_y$-$N_2O$ correlation observed inside the Arctic vortex in February 1997: Dynamical and chemical effects, *J. Geophys. Res.*, *104*, 8215–8224, 1999.

Kumer, J. B., et al., Comparison of correlative data with $HNO_3$ version 7 from the CLAES instrument deployed on the NASA Upper Atmosphere Research Satellite, *J. Geophys. Res.*, *101*, 9621–9656, 1996.

Lary, D. J., M. P. Chipperfield, J. A. Pyle, W. A. Norton, and L. P. Riishojgaard, Three-dimensional tracer initialization and general diagnostics using equivalent PV latitude-potential-temperature coordinates, *Q. J. R. Meteorol. Soc.*, *121*, 187–210, 1995.

Manney, G. L., and R. W. Zurek, Interhemispheric comparison of the development of the stratospheric polar vortex during fall: A 3-dimensional perspective for 1991–92, *Geophys. Res. Lett.*, *20*, 1275–1278, 1993.

Manney, G. L., R. W. Zurek, M. E. Gelman, A. J. Miller, and R. Nagatani, The anomalous Arctic lower stratospheric polar vortex of 1992–1993, *Geophys. Res. Lett.*, *21*, 2405–2408, 1994a.

Manney, G. L., et al., Chemical depletion of ozone in the Arctic lower stratosphere during winter 1992-93, *Nature*, *370*, 429–434, 1994b.

Manney, G. L., R. W. Zurek, A. O'Neill, and R. Swinbank, On the motion of air through the stratospheric polar vortex, *J. Atmos. Sci.*, *51*, 2973–2994, 1994c.

Manney, G. L., L. Froidevaux, J. W. Waters, and R. W. Zurek, Evolution of Microwave Limb Sounder ozone and the polar vortex during winter, *J. Geophys. Res.*, *100*, 2953–2972, 1995a.

Manney, G. L., et al., Formation of low ozone pockets in the middle stratospheric anticyclone during winter, *J. Geophys. Res.*, *100*, 13,939–13,950, 1995b.

Manney, G. L., R. W. Zurek, L. Froidevaux, J. W. Waters, A. O'Neill, and R. Swinbank, Lagrangian transport calculations using UARS data. Part II: Ozone, *J. Atmos. Sci.*, *52*, 3069–3081, 1995c.

Manney, G. L., M. L. Santee, L. Froidevaux, J. W. Waters, and R. W. Zurek, Polar vortex conditions during the 1995–96 Arctic winter: Meteorology and MLS ozone, *Geophys. Res. Lett.*, *23*, 3203–3206, 1996a.

Manney, G. L., R. Swinbank, and A. O'Neill, Stratospheric meteorological conditions for the 3–12 Nov 1994 ATMOS/ATLAS–3 measurements, *Geophys. Res. Lett.*, *23*, 2409–2412, 1996b.

Manney, G. L., L. Froidevaux, M. L. Santee, R. W. Zurek, and J. W. Waters, MLS observations of Arctic ozone loss in 1996–97, *Geophys. Res. Lett.*, *24*, 2697–2700, 1997.

Manney, G. L., J. C. Bird, D. P. Donovan, T. J. Duck, J. A. Whiteway, S. R. Pal, and A. I. Carswell, Modeling ozone laminae in ground-based Arctic wintertime observations using trajectory calculations and satellite data, *J. Geophys. Res.*, *103*, 5797–5814, 1998.

Michelsen, H. A., G. L. Manney, M. R. Gunson, C. P. Rinsland, and R. Zander, Correlations of stratospheric abundances of $CH_4$ and $N_2O$ derived from ATMOS measurements, *Geophys. Res. Lett.*, *25*, 2777–2780, 1998a.

Michelsen, H. A., G. L. Manney, M. R. Gunson, and R. Zander, Correlations of stratospheric abundances of $NO_y$, $O_3$, $N_2O$, and $CH_4$ derived from ATMOS measurements, *J. Geophys. Res.*, *103*, 28,347–28,359, 1998b.

Michelsen, H. A., et al., Intercomparison of ATMOS, SAGE II, and

ER-2 observations in Arctic vortex and extra-vortex air masses during spring 1993, *Geophys. Res. Lett.*, *26*, 291–294, 1999.

Morris, G. A., et al., Trajectory mapping and applications to data from the Upper Atmosphere Research Satellite, *J. Geophys. Res.*, *100*, 16,491–16,505, 1995.

Morris, G. A., S. R. Kawa, A. R. Douglass, M. R. Schoeberl, L. Froidevaux, and J. W. Waters, Low ozone pockets explained, *J. Geophys. Res.*, *103*, 3599–3610, 1998.

Mote, P. W., et al., An atmospheric tape recorder: The imprint of tropical tropopause temperatures on stratospheric water vapor, *J. Geophys. Res.*, *101*, 3989–4006, 1996.

Nair, H., M. Allen, L. Froidevaux, and R. W. Zurek, Localized rapid ozone loss in the northern winter stratosphere: An analysis of UARS observations, *J. Geophys. Res.*, *103*, 1555–1571, 1998.

Nedoluha, G. E., D. E. Siskind, J. T. Bacmeister, R. M. Bevilacqua, and J. M. Russell III, Changes in upper stratospheric $CH_4$ and $NO_2$ as measured by HALOE and implications for changes in transport, *Geophys. Res. Lett.*, *25*, 987–990, 1998a.

Nedoluha, G. E., R. M. Bevilacqua, R. M. Gomez, D. E. Siskind, B. C. Hicks, J. M. Russell III, and B. J. Connor, Increases in middle atmospheric water vapor as observed by the Halogen Occultation Experiment and the ground-based Water Vapor Millimeter-wave Spectrometer from 1991 to 1997, *J. Geophys. Res.*, *103*, 3531–3543, 1998b.

Newman, P. A., et al., Measurements of polar vortex air in midlatitudes, *J. Geophys. Res.*, *101*, 12,879–12,891, 1996.

Oltmans, S. J., and D. J. Hofmann, Increase in lower-stratospheric water vapor at a mid-latitude northern hemisphere site from 1981 to 1994, *Nature*, *374*, 146–149, 1995.

O'Neill, A., and V. D. Pope, The seasonal evolution of the extra-tropical stratosphere in the southern and northern hemispheres: Systematic changes in potential vorticity and the non-conservative effects of radiation, in *Dynamics, Transport and Photochemistry in the Middle Atmosphere of the Southern Hemisphere*, edited by A. O'Neill, pp. 33–54. Kluwer Acad., Norwell, Mass., 1990.

Pierce, R. B., T. D. Fairlie, W. L. Grose, R. Swinbank, and A. O'Neill, Mixing processes within the polar night jet, *J. Atmos. Sci.*, *51*, 2957–2972, 1994.

Plumb, R. A., D. W. Waugh, R. J. Atkinson, P. A. Newman, L. R. Lait, M. R. Schoeberl, E. V. Browell, A. J. Simmons, and M. Loewenstein, Intrusions into the lower stratospheric Arctic vortex during the winter of 1991–1992, *J. Geophys. Res.*, *99*, 1089–1105, 1994.

Pumphrey, H. C., Nonlinear retrievals of water vapour from the UARS Microwave Limb Sounder (MLS), *Adv. Space Res.*, *21*(3), 389–392, 1998.

Randel, W. J., and F. Wu, Climatology of stratospheric ozone based on SBUV and SBUV/2 data: 1978–1994, *Tech. Rep. NCAR/TN-412+STR*, Nat. Cent. for Atmos. Res., Boulder, Colo., 1995.

Randel, W. J., F. Wu, J. M. Russell III, A. E. Roche, and J. W. Waters, Seasonal cycles and QBO variations in stratospheric $CH_4$ and $H_2O$ observed in UARS HALOE data, *J. Atmos. Sci.*, *55*, 163–185, 1998.

Randel, W. J., F. Wu, J. M. Russell III, and J. W. Waters, Space-time patterns of trends in stratospheric constituents derived from UARS measurements, *J. Geophys. Res.*, *104*, 3711–3727, 1999.

Rinsland, C. P., M. R. Gunson, M. C. Abrams, L. L. Lowes, R. Zander, E. Mahieu, A. Goldman, and F. W. Irion, April 1993 Arctic profiles of stratospheric HCl, $ClONO_2$, and $CCl_2F_2$ from Atmospheric Trace Molecule Spectroscopy/ATLAS 2 infrared solar occultation spectra, *J. Geophys. Res.*, *100*, 14,019–14,027, 1995.

Rinsland, C. P., et al., ATMOS measurements of $H_2O + 2CH_4$ and total reactive nitrogen in the November 1994 Antarctic stratosphere: Dehydration and denitrification in the vortex, *Geophys. Res. Lett.*, *23*, 2397–2400, 1996a.

Rinsland, C. P., et al., ATMOS/ATLAS–3 measurements of stratospheric chlorine and reactive nitrogen partitioning inside and outside the November 1994 Antarctic vortex, *Geophys. Res. Lett.*, *23*, 2365–2368, 1996b.

Rinsland, C. P., et al., Polar stratospheric descent of $NO_y$ and CO and Arctic denitrification during winter 1992–1993, *J. Geophys. Res.*, *104*, 1847–1861, 1999.

Roche, A. E., et al., Validation of $CH_4$ and $N_2O$ measurements by the Cryogenic Limb Array Etalon Spectrometer instrument on the Upper Atmosphere Research Satellite, *J. Geophys. Res.*, *101*, 9679–9710, 1996.

Rosenfield, J. E., P. A. Newman, and M. R. Schoeberl, Computations of diabatic descent in the stratospheric polar vortex, *J. Geophys. Res.*, *99*, 16,677–16,689, 1994.

Ruth, S., R. Kennaugh, L. J. Gray, and J. M. Russell III, Seasonal, semiannual, and interannual variability seen in measurements of methane made by the UARS Halogen Occultation Experiment, *J. Geophys. Res.*, *102*, 16,189–16,199, 1997.

Santee, M. L., G. L. Manney, L. Froidevaux, W. G. Read, and J. W. Waters, Six years of UARS Microwave Limb Sounder $HNO_3$ observations: Seasonal, interhemispheric, and interannual variations in the lower stratosphere, *J. Geophys. Res.*, *104*, 8225–8246, 1999.

Schoeberl, M. R., et al., Reconstruction of the constituent distribution and trends in the Antarctic polar vortex from ER-2 flight observations, *J. Geophys. Res.*, *94*, 16,815–16,845, 1989.

Schoeberl, M. R., L. R. Lait, P. A. Newman, and J. E. Rosenfield, The structure of the polar vortex, *J. Geophys. Res.*, *97*, 7859–7882, 1992.

Schoeberl, M. R., M. Luo, and J. E. Rosenfield, An analysis of the Antarctic Halogen Occultation Experiment trace gas observations, *J. Geophys. Res.*, *100*, 5159–5172, 1995.

Strahan, S. E., J. E. Nielson, and M. C. Cerniglia, Long-lived tracer transport in the Antarctic stratosphere, *J. Geophys. Res.*, *101*, 26,615–26,629, 1996.

Sugita, T., et al., Denitrification observed inside the Arctic vortex in February 1995, *J. Geophys. Res.*, *103*, 16,221–16,233, 1998.

Sutton, R. T., H. MacLean, R. Swinbank, A. O'Neill, and F. W. Taylor, High-resolution stratospheric tracer fields estimated from satellite observations using Lagrangian trajectory calculations, *J. Atmos. Sci.*, *51*, 2995–3005, 1994.

Swinbank, R., and A. O'Neill, A stratosphere-troposphere data assimilation system, *Mon. Weather Rev.*, *122*, 686–702, 1994.

Vömel, H., M. Rummukainen, R. Kivi, J. Karhu, T. Turunen, E. Kyrö, J. Rosen, N. Kjome, and S. Oltmans, Dehydration and sedimentation of ice particles in the Arctic stratospheric vortex, *Geophys. Res. Lett.*, *24*, 795–798, 1997.

Waugh, D. W., and W. J. Randel, Climatology of Arctic and Antarctic polar vortices using elliptical diagnostics, *J. Atmos. Sci.*, *56*, 1594–1613, 1999.

Waugh, D. W., et al., Mixing of polar vortex air into middle latitudes as revealed by tracer-tracer scatterplots, *J. Geophys. Res.*, *102*, 13,119–13,134, 1997.

Zurek, R. W., G. L. Manney, A. J. Miller, M. E. Gelman, and R. M. Nagatani, Interannual variability of the north polar vortex in the lower stratosphere during the UARS mission, *Geophys. Res. Lett.*, *23*, 289–292, 1996.

M. R. Gunson, Jet Propulsion Laboratory, Mail Stop 169-237, Pasadena, CA 91109.

F. W. Irion, Jet Propulsion Laboratory, Mail Stop 183-601, Pasadena, CA 91109.

N. J. Livesey, G. L. Manney, and M. L. Santee, Jet Propulsion Laboratory, Mail Stop 183-701, Pasadena, CA 91109. (e-mail: manney@mls.jpl.nasa.gov)

H. A. Michelsen, Atmospheric and Environmental Research, Inc., 2682 Bishop Drive, Suite 120, San Ramon, CA 94583.

A. E. Roche, Lockheed Martin Advanced Technology Center, Org H1-11, Building 255, 3251 Hanover Street, Palo Alto, CA 94304.

(Received February 26, 1999; revised May 5, 1999; accepted May 7, 1999.)